

Astrophysical and cosmological evidence for dark matter and dark energy

Marco Roncadelli*

INFN – Pavia, via A. Bassi 6, 27100 – Italy

E-mail: marco.roncadelli@pv.infn.it

Assuming that known physical laws hold true throughout the Universe, I first discuss the observational evidence for dark matter in galaxies and their clusters. Next, I analyze the cosmological relevance of these results. Finally, I combine this information with cosmological observations to draw conclusions about the amount and nature of the dark matter and dark energy in the Universe.

*XVI International Workshop on Neutrino Telescopes,
2-6 March 2015
Palazzo Franchetti — Istituto Veneto, Venice, Italy*

*Speaker.

1. Introduction

Almost all information about the Universe is carried by photons. And it is obvious that we miss most of the photons emitted by the astronomical objects. Therefore, most of the matter in the Universe is dark. So, why bother? In fact, people did not, until it became compelling to believe that the bulk of the dark matter must be *totally different* in nature from the luminous one.

Such a dramatic result came about by combining the theory of galaxy formation with the observations of the cosmic microwave background (CMB), and requires that the Universe is dominated by the so-called *cold non-baryonic dark matter* – cold dark matter (CDM) for short – consisting of some new kind of neutral and effectively stable elementary particle which is non-relativistic when it decouples from the rest of the matter as the Universe expands and cools. Quite remarkably, elementary-particle physics offers many realistic candidates for CDM – neutralinos, axions, etc. – even if none of them has been detected so far. Equally remarkable is the fact – often not sufficiently appreciated – that the CDM scenario is in agreement with the observational lack of luminous matter in galaxies and their clusters, since otherwise there would be no room for CDM. Indeed, such a “missing mass” should be just CDM.

Surprisingly – even by taking CDM into account – consistency with cosmological observations also concerning the CMB leads to the conclusion that about 70% of the stuff present in the Universe is missing. The way out of this conundrum came in 1997, when it was discovered that the present cosmic expansion is accelerated. Clearly, in order for the expansion to be accelerated gravity must become repulsive over cosmic scales. This can happen within general relativity provided that some sort of stuff with positive energy like luminous matter and CDM but with negative pressure dominates. Such a stuff generating repulsive gravity is also self-repulsive, and so it should be uniformly spread throughout the Universe without making structures: in the lack of any idea about its nature it has been called *dark energy*. By employing Type Ia supernovae as *standard candles*¹ it has been shown that the amount of dark energy is just right to fill the gap.

In conclusion, while nowadays we have a precise and consistent inventory of the various forms of invisible stuff, their physical nature still remains elusive. It is certainly frustrating that about 95% of what is out there is something that we have not even the slightest idea about.²

It will be assumed throughout this Proceeding that gravity is described by Einstein field equations.

2. Astrophysical approach

Basically, two completely different methods are used to discover the presence of dark matter and quantify its amount in galaxies and their clusters.

¹Consider an astronomical effectively point-like object that emits isotropically in empty space, and denote by L its absolute luminosity. It is well known that the observed flux at distance r is given by $F(r) = L/(4\pi r^2)$. Usually, by determining both $F(r)$ and r one obtains L . However, for certain well studied astronomical objects one can estimate L without using the above procedure. For instance, for Cepheid variable stars, one can infer L by measuring their period. Objects of this kind are called *standard candles*, since from the knowledge of L and $F(r)$ one can derive the distance r .

²We recall that the amount of baryons is less than 5%.

2.1 Dynamical analysis

It relies upon the gravitational effect produced by dark matter on the luminous mass. More precisely, the existence and morphology of dark matter is estimated from a careful dynamical analysis of some suitably chosen astronomical object called *mass tracer*, and often a set of mass tracers is employed.

A brief historical sketch of the dynamical analysis is enlightening. It was started by the great mathematician Bessel in 1844, when he studied the orbit of Sirius, the brightest star in the sky. Needless to say, his expectation was that it ought to be elliptical. However, he found that in reality it exhibits small fluctuations about an ellipse. His interpretation was that there should be some hidden astronomical object nearby that perturbs Sirius orbit. Owing to his mathematical skillness, he was able to determine the position of the perturber, which soon thereafter was discovered by means of a pointed observation: it has become known as Sirius B, which is a white dwarf. In this example, Sirius plays the rôle of mass tracer, while Sirius B that of dark matter. Just two years later, Adams and Le Verrier independently observed the orbit of Uranus, and again noted that it slightly fluctuates about an ellipse. On the wake of Bessel's discovery, they supposed that the small perturbations are brought about by a hidden astronomical object. Again its position was calculated, and by a pointed observation the perturber was found to be the planet Neptune. As before, Uranus is the tracer, whereas Neptune is the dark matter. Only in 1915 was the dynamical analysis applied to the Milky Way. Specifically, Öpik asked the question whether there is some dark matter in our neighborhood. To this end he studied the vertical motion of stars in the considered region. Since they respond to the *total* gravitational mass in the disk, from this kind of observations one can infer whether the total mass in our neighborhood exceeds the luminous one – whose amount can be evaluated by star counts – in which case there would be positive evidence for the existence of local dark matter. His conclusion was that no dark matter exists. A subsequent step was taken in 1922 by Kapteyn (who coined the word *dark matter*) [1] and in 1922-1923 by Jeans [2, 3], considering again the vertical motion of stars. However, while Kapteyn treated stars incorrectly – like Öpik – as collisional objects, Jeans considered them correctly as collisionless ones. Kapteyn reached basically the same conclusion of Öpik, while Jeans found that the existence of dark matter is quite likely and its amount can be twice as large as that of stars. A more careful treatment along the same lines was performed in 1932 by Oort, who found that the local dark matter density is $\rho_{\text{dark}} \simeq 2.05 (\text{GeV}/c^2) \text{cm}^{-3}$ [4]. In a subsequent reanalysis which included also the gas contribution in 1960 Oort found $\rho_{\text{dark}} \simeq 2.66 (\text{GeV}/c^2) \text{cm}^{-3}$ [5]. In all these examples stars in vertical motion clearly form the set of mass tracers. This problem is deceptively simple, and it has been the subject of hot debates for decades. Only recently a general agreement has been achieved, leading to $0.2 (\text{GeV}/c^2) \text{cm}^{-3} < \rho_{\text{dark}} < 0.6 (\text{GeV}/c^2) \text{cm}^{-3}$ [6]. Incidentally, this quantity is of crucial importance for all direct underground dark matter searches.

A different approach was pursued in 1933 by Zwicky, who applied for the first time the virial theorem to the Coma cluster of galaxies, which is the archetype of a regular galaxy cluster. As is well known, the virial theorem tells that twice the average kinetic energy plus the average potential energy is zero provided that the system is in equilibrium. As far as Coma is concerned, the latter condition is certainly met because the time needed by a generic galaxy to cross the cluster is much shorter than the presumed age of Coma. This means that Coma must have reached an equilibrium

configuration, otherwise its galaxies would have fled apart since a long time. By measuring the line-of-sight velocity of 7 galaxies – taking them as representative for the whole galaxy population – Zwicky came to the result that the potential energy is by a factor of order 400 larger than the contribution of galaxies similar to the field galaxies in our neighborhood. Thus, he concluded that on average each Coma galaxy should contain an amount of dark matter roughly 400 larger than that of luminous mass, assuming that the fraction of dark matter in our neighboring galaxies is negligible as compared with luminous mass (we shall repeat this exercise below) [7]. It must be said, though, that in a more detailed analysis of this problem in 1937, Zwicky withdrew his original suggestion of dark matter and explained the huge value of the mass of the Coma galaxies by arguing that cluster galaxies should be much more massive than field galaxies because of a very efficient merging [8].

We shall be much more specific about the application of the dynamical analysis when its applications will be addressed.

2.2 Gravitational lensing

According to general relativity, any mass distribution makes the surrounding tridimensional space curved. As a consequence, any light ray that passes close enough to a mass clump follows a highly nontrivial null geodesic, and so gravitational lensing can magnify, distort and multiply the images of background sources [9].

It looks rather strange in retrospect that Einstein did not recognize its importance, even when the amateur astronomer Mandl urged him to investigate the problem. Quite likely – more to make Mandl happy than for his own true belief – Einstein published in 1936 a short paper on gravitational lensing in which both a background star (source) and a foreground one (lens) lie along the same line of sight [10]. He found that the image is a perfect circle, the so-called *Einstein ring*, and since the specific intensity is conserved, the whole surface brightness of the source gets squeezed into the Einstein ring, which is therefore much brighter than an ordinary star (we shall repeat this exercise below). Yet, Einstein was quite skeptical that such phenomenon could ever be seen, given the vanishingly small probability of such a perfect alignment. Just one year later, Zwicky considered the same configuration, replacing however stars by galaxies. He immediately noted that in this case the probability of observing gravitational lensing becomes much larger than in the case of stars [11]. Soon thereafter, he claimed that such a probability actually becomes a certainty, provided that the lens is a cluster galaxy with the estimated mass that he previously obtained for Coma [12].

We neglect for simplicity cosmological effects and work in flat space, so that the background metric is that of Minkowski. Any application of gravitational lensing considered in this Proceeding is based on the *thin-lens approximation*, according to which the typical size of the lens $D_{\mathcal{L}}$ is much smaller than all involved distances. One of the several consequences of such an approximation – which is always met for galaxies and their clusters – is that the whole resulting gravitational effect on light rays is simply embodied in a *refraction index* of the form

$$n(\mathbf{x}) = 1 - \frac{2\Phi(\mathbf{x})}{c^2}, \quad (2.1)$$

where $\Phi(\mathbf{x})$ is the newtonian potential ($|\Phi(\mathbf{x})| \ll c^2$). So, we see that a mass clump acts exactly like a normal lens as far as the images of background luminous objects are concerned. Moreover – at variance with ordinary optics – gravitational lensing is frequency-independent, or *achromatic*.

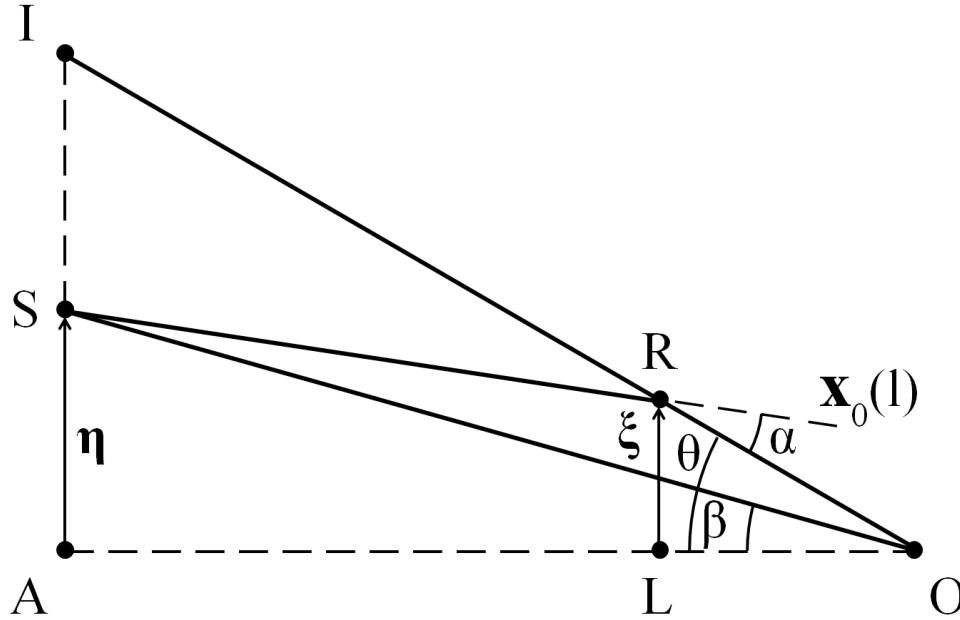


Figure 1: Typical lensing situation.

Let us now sketch a typical lensing situation. An optical ray emitted by a point S of an extended source \mathcal{S} gets deflected of an angle α by an extended lens \mathcal{L} whose centre-of-mass (CM) lies in L before reaching the observer \mathcal{O} in O : this is the *lensed* optical ray $\mathbf{x}(t)$. We denote throughout the present discussion by \mathcal{I} either the observed single image of \mathcal{S} or a generic component of a multiple image, and by I the observed image of S or a component of a multiple image thereof. Lensing implies that I is in a position *different* from S . The straight line joining O with L is called the *optical axis*, the plane perpendicular to the optical axis through L is named the *lens plane* while the plane perpendicular to the optical axis through S is called the *source plane*. We denote by θ the angular position of I – or of a single component of a multiple image – with respect to the optical axis, and similarly by β the angular position of S ³. Letting A be the projection of S on the optical axis, we denote by η the distance of S from A in the source plane, and by ξ the distance of $\mathbf{x}(l)$ from L in the lens plane. We stress that unless \mathcal{L} is symmetric about the optical axis the point I does *not* belong in general to the plane defined by the points S , L and O , so that I can have an *arbitrary* position.

All this is shown in Figure 1 for a single image for simplicity, but the same construction can be applied to every component of a multiple image. We let R be the point where $\mathbf{x}(l)$ as emitted by S crosses the lens plane. Because in general the point I does not belong to the plane defined by the

³Clearly these angles are represented by two-dimensional vectors.

points S , L and O , Figure 1 is generally the *projection* of the real geometric setting onto the latter plane.

Note that at this stage the thin-lens approximation can be formalized as $D_{\mathcal{L}} \ll \overline{OL}$ and $D_{\mathcal{L}} \ll \overline{LS}$, besides the previous assumption that the gravitational field produced by \mathcal{L} is weak enough. It is easy to show that in such a situation all involved angles are very small, and so we will assume throughout our discussion $\alpha \ll 1$, $\beta \ll 1$ and $\theta \ll 1$.

As a matter of fact, the thin-lens approximation possesses two further implications.

- Gravitational lensing is effective only in a very small region surrounding \mathcal{L} and in fact can be thought to occur *instantaneously* and *only* in the lens plane (namely at the point R), so that the lensed optical ray $\mathbf{x}(l)$ can be approximated to a very good accuracy by the broken line SRO even if in reality it is a smooth curve close to \mathcal{L} .
- Owing to the smallness of α , β and θ , $\mathbf{x}(l)$ and the *unperturbed* optical ray $\mathbf{x}_0(l)$ are nearly orthogonal to the source and the lens planes. In order to avoid misunderstandings, we stress the difference between the unlensed and the unperturbed optical rays. The former is the ray emitted by S which reaches \mathcal{O} in the absence of \mathcal{L} . The latter is the ray emitted by S in the *same* direction of the ray $\mathbf{x}(l)$ that reaches \mathcal{O} because of lensing (straight line SR in Figure 1). Note that the unperturbed ray does *not* cross \mathcal{O} . So, both $\mathbf{x}(l)$ and $\mathbf{x}_0(l)$ have the same tangent unit vector $\hat{\mathbf{e}}_S$ at S , which in first approximation is *normal* to the source and the lens planes.

Deflection angle: An advantage of the thin-lens approximation is that the deflection angle $\alpha(\xi)$ can be straightforwardly evaluated as in geometric optics starting from the Fermat principle

$$\delta \int_O^S dl n(\mathbf{x}(l)) = 0, \quad (2.2)$$

where $n(\mathbf{x})$ is given by Eq. (2.1) and δ denotes an arbitrary variation – vanishing at the end points – of the arbitrary smooth parametrized path $\mathbf{x}(l)$ joining O and S . The result is

$$\alpha(\xi) = \frac{4G}{c^2} \int_S^O d^2 \xi' \frac{\xi - \xi'}{|\xi - \xi'|^2} \Sigma(\xi'), \quad (2.3)$$

where $\Sigma(\xi)$ is the density of \mathcal{L} as projected onto the plane of the sky: the independence of the tridimensional lens density $\rho(\mathbf{x})$ is another consequence of the thin-lens approximation. So, turning the argument around, gravitational lensing allows only for the determination of $\Sigma(\xi)$ but not of $\rho(\mathbf{x})$ from observations.

Lens equation: The three angles α , β and θ are not independent, but they are related by the lens equation. Basically, the lens equation arises by representing the vector \mathbf{SI} in two different ways. One is $\mathbf{SI} = (\theta - \beta)\overline{OS}$, while the other reads $\mathbf{SI} = \alpha(\xi)\overline{RS}$. Upon their equality and the replacement $\overline{RS} \rightarrow \overline{LS}$, we get

$$\beta = \theta - \alpha(\xi) \frac{\overline{LS}}{\overline{OS}}. \quad (2.4)$$

In view of our purposes, we better rewrite Eq. (2.4) in terms of $\boldsymbol{\eta}$ and $\boldsymbol{\xi}$. This goal is easily achieved by inserting $\boldsymbol{\eta} = \boldsymbol{\beta} \overline{OS}$ and $\boldsymbol{\theta} = \boldsymbol{\xi} / \overline{OL}$ into the latter equation, thereby obtaining

$$\boldsymbol{\eta} = \boldsymbol{\xi} \frac{\overline{OS}}{\overline{OL}} - \boldsymbol{\alpha}(\boldsymbol{\xi}) \overline{LS}. \quad (2.5)$$

Even if the angle $\boldsymbol{\beta}$ and the distance $\boldsymbol{\eta}$ are not observable since we cannot remove the lens, we shall see that the lens equation plays a fundamental rôle in the astrophysical applications of gravitational lensing.

It looks quite instrumental for our subsequent analysis to consider a lens which is *axially symmetric* about the optical axis and a *point-like* source just on the optical axis. In such a situation, it can be shown that the deflection angle lies along the vector $\boldsymbol{\xi}$. Specifically, we have

$$\boldsymbol{\alpha}(\boldsymbol{\xi}) = \frac{4GM(\boldsymbol{\xi})}{c^2 \xi^2} \boldsymbol{\xi}, \quad M(\boldsymbol{\xi}) \equiv 2\pi \int_0^\xi d\xi' \xi' \Sigma(\xi'), \quad (2.6)$$

so that the lens equation (2.5) becomes one-dimensional and reads⁴

$$\left(\frac{\overline{OS}}{\overline{OL}} - \frac{4GM(\boldsymbol{\xi}) \overline{LS}}{c^2 \xi^2} \right) \boldsymbol{\xi} = 0. \quad (2.7)$$

Suppose first that the lens has constant surface density equal to its critical density $\Sigma_{\text{cr}} \equiv c^2 \overline{OS} / (4\pi G \overline{OL} \overline{LS})$, which yields $M(\boldsymbol{\xi}) = \pi \Sigma_{\text{cr}} \xi^2$. Hence the lens equation (2.7) degenerates into $0 \cdot \boldsymbol{\xi} = 0$. Manifestly, this means that *all rays* emitted by \mathcal{S} get focalized onto \mathcal{O} .

Consider now the previously discussed configuration envisaged by Einstein, namely a point-like \mathcal{L} of mass M on the line of sight to a point-like \mathcal{S} . Accordingly, we have $\Sigma(\boldsymbol{\xi}) = M \delta^2(\boldsymbol{\xi})$, which yields $M(\boldsymbol{\xi}) = M$, leading in turn to the following lens equation

$$\left(\frac{\overline{OS}}{\overline{OL}} - \frac{4GM \overline{LS}}{c^2 \xi^2} \right) \boldsymbol{\xi} = 0. \quad (2.8)$$

Because the lens is opaque, the solution $\boldsymbol{\xi} = 0$ has to be discarded, so that Eq. (2.8) gives

$$\xi_E = \left(\frac{4GM \overline{OL} \overline{LS}}{c^2 \overline{OS}} \right)^{1/2}, \quad (2.9)$$

which is called *Einstein radius*. So, \mathcal{O} will see the image \mathcal{I} of \mathcal{S} as a perfect ring – the Einstein ring – of radius ξ_E .

Owing to our subsequent applications, we have to distinguish between two quite different situations.

A. Strong lensing

This phenomenon concerns only *regular* clusters and some massive galaxies. It is characterized by the existence of *giant arcs* inside the image of the lens. Let us now discuss how these giant arcs arise and how they can be used to estimate the lens mass [13].

⁴In this case, Figure 1 represents the real situation.

In order to be specific, we consider regular clusters, but as we said the same strategy applies also to massive galaxies. First of all, we recall that regular clusters possess *spherical symmetry* at least in first approximation, which means *axial symmetry* about the optical axis. Let us first address the situation in which \mathcal{L} is a regular cluster and the \mathcal{S} is a point-like source as a star. Accordingly, it can be shown that \mathcal{O} sees \mathcal{S} as an Einstein ring whenever the average surface density $\overline{\Sigma(\xi_E)} \equiv M(\xi)/(\pi \xi^2)$ equals the critical density Σ_{cr} . Whence

$$M(\xi_E) = \frac{c^2}{4\pi G} \frac{\overline{OS}}{\overline{OLS}} \xi_E^2 = \pi \Sigma_{\text{cr}} \xi_E^2. \quad (2.10)$$

So, we see that by measuring the Einstein radius and knowing \overline{OL} , \overline{LS} and \overline{OS} we immediately find the lens mass enclosed by the Einstein radius.

Suppose next that the star is replaced by a galaxy, namely an extended \mathcal{S} . It can be shown that in such a situation \mathcal{S} becomes a pair of oppositely-located giant arcs which are sectors of the Einstein ring, but Eq. (2.10) retains its validity.

Suppose finally that the axial symmetry is slightly perturbed. Then one of the two arcs is greatly demagnified whereas the other is not – which is very bright because it contains the whole galaxy luminosity – and in first approximation Eq. (2.10) is still valid. As a result, by determining the distances of the lens and the source – and the Einstein radius traced by the giant arc – we are able to determine the cluster mass enclosed by ξ_E .⁵

Let us address the main limitations of this technique. First of all, the formation of giant arcs requires the nearly perfect alignment of O , L and S , which is clearly a very unlikely situation. Finally, only the mass inside the Einstein ring can be estimated in this way [13].

B. Weak lensing

Every cluster or massive galaxy acts as a lens \mathcal{L} , producing *weakly distorted* images \mathcal{I} of all background galaxies \mathcal{S} whose *projected* position lies close enough to its position on the sky, while their distance along the line of sight is *arbitrary* and does not matter at all. It can be shown that in general weak lensing *squeezes* \mathcal{I} along the *radial* projected direction – namely that joining the I to L – while *stretching* the image along the *tangential* projected direction, which is orthogonal to the above radial direction. As a result, the image of a round background galaxy becomes elliptical, and that of an elliptical galaxy acquires a larger observed ellipticity. Hence, these images are called *arclets* [14].

Now, if the background galaxy population were fully made of round galaxies alone, the observed ellipticity of every arclet would tell us how strong is the gravitational field at any arclet position, from which the cluster mass reconstruction would be straightforward. Unfortunately, life is not that easy, since we know that background unlensed elliptical galaxies have an unknown intrinsic ellipticity. So, the knowledge of the ellipticity of a single corresponding arclet is useless. Still, this trivial remark naturally suggests the way towards a successful achievement. Indeed, suppose to contemplate *many* background galaxies at once. Since their position along the line of sight is arbitrary, they are certainly uncorrelated, which implies in turn that their individual ellipticities

⁵The source distance is determined through the redshift of \mathcal{S} – which is obviously the same as that of \mathcal{L} – since \mathcal{S} is typically at a cosmological distance.

are uncorrelated as well, and so manifestly randomly oriented. Therefore – in the absence of weak lensing – their intrinsic average ellipticity vanishes, and of course the same is true for their images. Yet, owing to the above properties of weak lensing, the average ellipticity of the corresponding arclets – which is called the *polarization* – directly quantifies the weak lensing effect, which is obviously proportional to the cluster surface density $\Sigma(\xi)$, and so ultimately allows to determine it.

Finally, an important remark is in order. At variance with other methods to determine the cluster mass determination, this does *not* require any assumption about the dynamical state of the cluster.

2.3 Mass-to-light ratios

A concept of paramount importance for the discussion of dark matter is that of mass-to-light ratio.

Consider first an astronomical object made of *luminous* matter alone. Then we define the associated *luminous* mass-to-light ratio as

$$\Upsilon_{\text{lum}} \equiv \frac{M_{\text{lum}}}{L} \Upsilon_{\odot}. \quad (2.11)$$

The masses of galaxies and their clusters are currently expressed in terms of the solar mass $M_{\odot} = 1.99 \cdot 10^{33}$ g, and likewise their luminosities in terms of the Sun luminosity $L_{\odot} = 3.84 \cdot 10^{33}$ erg s⁻¹. So, it is natural to express Υ_{lum} in units of $\Upsilon_{\odot} \equiv M_{\odot}/L_{\odot}$, with the obvious understanding that in Eq. (2.11) both M_{lum} and L are dimensionless numbers in the considered units. For instance, since for main-sequence stars – which contain no dark matter – we have on average $L/L_{\odot} = (M_{\text{lum}}/M_{\odot})^{3.5}$, Eq. (2.11) entails $\Upsilon_{\text{lum}} = M_{\text{lum}}^{-2.5} \Upsilon_{\odot}$, with M_{lum} expressed in solar units.

* * *

Now, the crux of the argument is that even if galaxies contain quite a lot of dark matter as we shall see, nonetheless the value of Υ_{lum} can be evaluated by means of stellar population synthesis models, without any need for observations. As is well known, according to Hubble, galaxies are classified as ellipticals (E), lenticulars (S0), spirals (Sa, Sb, Sc, with the size of the bulge decreasing from Sa to Sc) and irregulars (Irr). Accordingly, the average values of Υ_{lum} are reported in Table 1.

Table 1

Y	$\langle \Upsilon_{\text{lum},B} \rangle_Y / \Upsilon_{\odot,B}$
E	6.5
S0	4.7
Sa	3.2
Sb	2.3
Sc	1.8
Irr	1.1

* * *

Suppose now that an astronomical objects contains both luminous and dark matter, as we shall see to be the case of galaxies and clusters. In such a situation, we also define a *total* mass-to-light ratio as

$$\Upsilon \equiv \frac{M}{L} \Upsilon_{\odot}, \quad (2.12)$$

where M is the total dynamical mass, namely the sum of M_{lum} and M_{dark} (as before M and L are supposed to be expressed in solar units).

We stress that it is of paramount importance to keep the two mass-to-light ratios Υ_{lum} and Υ sharply distinct. In fact, since $\Upsilon/\Upsilon_{\text{lum}} = M/M_{\text{lum}}$ it follows that the ratio $\Upsilon/\Upsilon_{\text{lum}}$ yields the ratio of the total-to-luminous mass present in a galaxy or in a cluster. As it will become clear later, often it turns out to be more convenient to use Υ_{lum} and Υ rather than M_{lum} and M , respectively, in order to quantify the amount of luminous and dark matter in the considered system, since the luminosity is always supposed to be a known quantity.

In general both Υ_{lum} and Υ are expressed in terms of the luminosity in the *visual* (V) or *blue* (B) band. Finally, it goes without saying that it will be crucial to keep the two mass-to-light ratios sharply distinct if we are to avoid misunderstandings.

3. Astrophysical evidence of dark matter

Because CDM plays an essential rôle in the process of galaxy formation, a natural expectation is that it should be found in galaxies and their clusters. So, we proceed to investigate this issue in detail.

* * *

Before starting our real discussion, we point out that according to the Hubble classification galaxies consist – apart from irregulars – of two basic structure: the *Bulge* and the *Disk*. The bulge is a spheroidal structure made of old stars only. Disks are more complex objects, containing stars and cold atomic and molecular hydrogen clouds, often hosting a strong activity of star formation. Specifically, the situation is summarized as follows.

Ellipticals (E): They entirely consist of the bulge, which is of a spheroidal form as seen in projection.

Lenticulars (S0): They are made of a disk dominated by a very large spheroidal central bulge.

Spirals (Sa, Sb, Sc): They consist of disks with a central spheroidal bulge, whose size decreases along the sequence $\text{Sa} \rightarrow \text{Sc}$.

These qualitative statements have been quantified in 1985 by Kent in terms the average ratio $\mathcal{B}_{Y,B}$ of the fraction of the bulge luminosity over the total luminosity for elliptical, lenticular and spiral [15]. Their values are reported in Table 2.

Table 2

Hubble type Y	$\mathcal{B}_{Y,B}$
E	1
S0	0.64
Sa	0.33
Sb	0.16
Sc	0.061

Furthermore, population synthesis models predict the mass-to-light values for bulges, disks and irregulars. They are reported neglecting errors in Table 3.

Table 3

Y	$\langle Y_{*,B} \rangle_Y / Y_{\odot,B}$
Bulges	6.5
Disks	1.5
Irr	1.1

It is a simple exercise to obtain the values listed in Table 1 from those reported in Table 2 and Table 3.

3.1 Spiral galaxies

Spiral galaxies are the easiest ones to discover evidence for dark matter. The stellar disk has an exponential optical surface brightness profile

$$I_{\text{opt}}(R) \propto e^{-R/R_d}, \quad (3.1)$$

where R is the galactocentric distance and R_d denotes the *disk scale length*. Typically, it is found $2 \text{ kpc} < R_d < 4 \text{ kpc}$ and the disk *optical radius* turns out to be $R_{\text{opt}} \simeq 4R_d$. The stellar disk coexists with a gaseous disk, mostly made of cold neutral hydrogen (HI) clouds, whose radius is generally twice as large as compared to that of the stellar disk. Both stars and cold HI clouds travel on nearly *circular* orbits around the galactic centre with velocity $v_c(R)$, and so their centripetal acceleration equals the gravitational one

$$\frac{v_c^2(R)}{R} = -g_R(R, 0). \quad (3.2)$$

Hence, the *rotation curve* – namely the plot of v_c versus R – traces the gravitational acceleration in the disk $g_R(R, 0)$. This fact lies at the basis of the best strategy to uncover dark matter in spiral galaxies.

A. Rotation curve

Basically, a rotation curve is constructed by measuring the circular velocity – at different values of R – through the Doppler shift, either of certain optical spectral lines of stars or of the

line at 21 cm in the radio band emitted by HI clouds. We recall that the 21 cm line is due to the transition from the upper to the lower hyperfine level in which the non-relativistic ground state is split because of the interaction between the electron and proton magnetic moments, and the higher level is populated because the temperature of the interstellar medium is definitely larger than the energy gap between the hyperfine levels. The *observed* rotation curve of a given spiral is then compared with the one ideally produced by *luminous* matter alone: a discrepancy would be a clear-cut signal of dark matter.

Let us consider first the rotation curve arising solely from *luminous* matter, whose evaluation proceeds as follows. In the first place, the surface brightness profile – as given by Eq. (3.1) with R_d fixed by a photometric fit – has to be converted into the disk surface density profile $\Sigma(R)$. Because color and luminosity gradients in spiral disks are generally modest, the luminous mass-to-light ratio of the disk Υ_{lum} can be taken as *constant*. Accordingly, we get $\Sigma(R) \propto \Upsilon_{\text{lum}} I_{\text{opt}}(R)$, and so Eq. (3.1) entails

$$\Sigma(R) \propto e^{-R/R_d}, \quad (3.3)$$

It can next be shown that this mass distribution produces the following rotation curve

$$v_c(R) \propto \left[I_0\left(\frac{R}{2R_d}\right) K_0\left(\frac{R}{2R_d}\right) - I_1\left(\frac{R}{2R_d}\right) K_1\left(\frac{R}{2R_d}\right) \right]^{1/2} R, \quad (3.4)$$

where $I_0(\cdot)$, $I_1(\cdot)$, $K_0(\cdot)$ and $K_1(\cdot)$ are modified Bessel functions [16]. Although Eq. (3.4) looks complicated, its qualitative behavior is very simple: a *linear rise* in the inner region continues until a maximum is reached at $R = 2.2R_d$, which is followed by a *keplerian fall-off* at larger galactocentric distances. To a good approximation, Eq. (3.4) can be rewritten as

$$v_c(R) \sim \begin{cases} R, & R < R_d \\ R^{-1/2}, & R > 3R_d. \end{cases} \quad (3.5)$$

What is the information provided by *observations*? The systematic analysis of the *optical* rotation curves of spiral galaxy started in 1980 by Rubin and collaborators [17, 18, 19, 20, 21]. In spite of the fact that it is virtually impossible to find identical rotation curves, their result was astonishing, since the rotation curves of all considered galaxies share the *same* qualitative behavior: they *rise linearly* in the inner region until a maximum is reached close to $R = 2R_d$, beyond which they stay *flat* out to the last measured point to within 10%. This conclusion has been confirmed by subsequent optical observations [22, 23]. Schematically

$$v_c(R) \sim \begin{cases} R, & R < R_d \\ \text{constant}, & R > 3R_d. \end{cases} \quad (3.6)$$

Apparently, in the outer region $R > 3R_d$ the disagreement between the expectation based on luminous matter alone and observations is great. Still, such a conclusion should be understood more like as a strong suggestion than a real proof. Indeed, the considered method is – just by definition – bound to probe the optical region, namely $R < 4R_d$, and in fact the above analysis by Rubin and collaborators has been carried out up to $R \simeq 3.5R_d$. Unfortunately, Eq. (3.4) implies that at $R = 3.5R_d$ the circular velocity of luminous matter has decreased only by 8% relative to its

maximum at $R = 2.2R_d$. So, it is very difficult to rule out the keplerian fall-off by restricting the attention to the optical region.

Quite remarkably, radio observations have settled the issue [24, 25]. As we said, HI clouds typically extend out to *twice* the optical radius, thereby allowing for the determination of $v_c(R)$ out to $R \simeq 8R_d$, and in some cases farther out. In this way it has been show that the result in Eq. (3.6) actually retains its validity out to the edge of the gaseous disk, thereby providing a clear-cut evidence against the keplerian behavior. A beautiful example concerns the Sc spiral galaxy NGC 3198, whose rotation curve has been mapped out to $R \simeq 10R_d \simeq 30\text{kpc}$ [26].

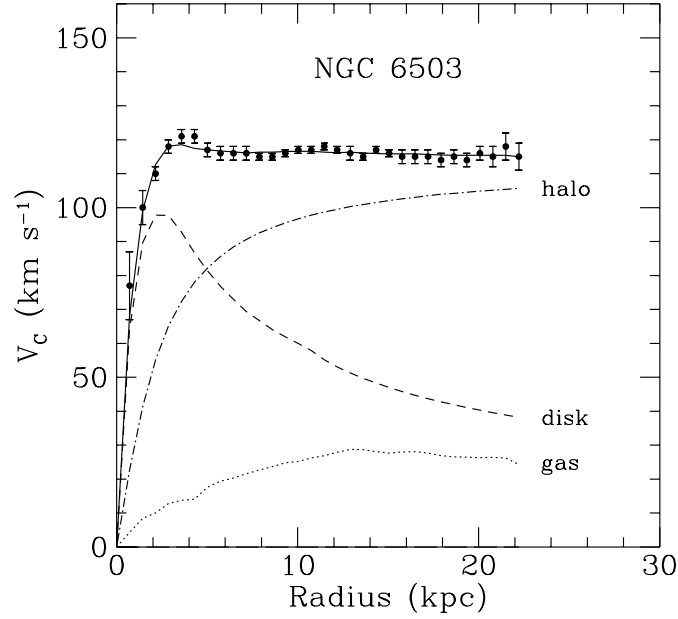


Figure 2: Rotation curve of NGC 3198.

In order to find out the meaning of the observations, let us compare Eqs. (3.6) and (3.5). As far as the inner region $R < R_d$ is concerned, the agreement is good, thereby implying that here luminous matter is the whole story. But in the outer region $R > 3R_d$ the disagreement is dramatic, with the circular velocity systematically larger and larger than expected on the basis of luminous matter alone as R increases. Actually, for fixed R a larger v_c implies by Eq. (3.2) a bigger g_R , which entails in turn by the Poisson equation (see below) a larger mass density ρ . Consequently, *dark matter must lurk* at galactocentric distances $R > 3R_d$.

Clearly, the flat behavior of the observed rotation curves provides solid evidence that the outer region of spiral galaxies is dominated by dark matter. This turns out to be a *universal* properties of spiral galaxies.

All these results hold true for the so-called high surface brightness spirals, which show a remarkable property: all their rotation curves fit within the *universal rotation curve*, which is uniquely fixed in terms of the luminosity L_B of the considered spiral [28, 29].

Yet, the actual shape of the dark matter distribution *cannot* be unambiguously determined from the rotation curve alone. This is true even under the simplifying assumption that such a distribution – just like the one of luminous matter – is *axisymmetric* about the galaxy rotation axis. Indeed, by employing cylindrical coordinates (R, ϕ, z) , the gravitational acceleration in a generic point $\mathbf{g}(R, z)$ is related to the mass density $\rho(R, z)$ by the *Poisson equation*

$$\frac{1}{R} \frac{\partial}{\partial R} \left(R g_R(R, z) \right) + \frac{\partial g_z(R, z)}{\partial z} = -4\pi G \rho(R, z). \quad (3.7)$$

Owing to Eq. (3.2), the rotation curve merely fixes $g_R(R, 0)$, and so the lack of knowledge about $g_R(R, z)$ with $z \neq 0$ and $g_z(R, z)$ prevents an unique determination of $\rho(R, z)$. *Only* by assuming that the dark matter distribution has *spherical symmetry* about the galaxy centre can the dark matter density profile $\rho(r)$ be *uniquely* derived from the rotation curve. To see this, consider the Poisson equation which now reads ⁶

$$\frac{1}{r^2} \frac{d}{dr} \left(r^2 g_r(r) \right) = -4\pi G \rho(r). \quad (3.8)$$

So, upon integration we get

$$g_r(r) = -\frac{GM(r)}{r^2}, \quad (3.9)$$

where $M(r)$ denotes throughout this Proceeding the *integrated mass profile*

$$M(r) \equiv 4\pi \int_0^r ds s^2 \rho(s), \quad (3.10)$$

namely the total mass inside the sphere of radius r . Combining Eqs. (3.2) and (3.9), we find

$$M(r) \propto v_c^2(r) r. \quad (3.11)$$

So, in the region where the observed rotation curve is *flat* eq. (3.11) becomes

$$M(r) \propto r, \quad (3.12)$$

and so Eq. (3.10) implies

$$\rho(r) \propto r^{-2}, \quad (3.13)$$

which is called an *isothermal profile*, since it is the same as the density profile of a *singular isothermal sphere* (SIS) ⁷. Thus, we come to the conclusion that spiral galaxies are surrounded by an isothermal halo *dominated* by dark matter. Within such scenario, optical observations typically show that $M_{\text{dark}}(R_{\text{opt}}) \simeq M_{\text{lum}}(R_{\text{opt}})$, whereas in the case of NGC 3198 radio observations yield $M_{\text{dark}}(30 \text{ kpc}) \simeq 16 M_{\text{lum}}$. However, one should not forget that this conclusion rests on the simple but unproved assumption of spherical symmetry.

⁶Notationally, we denote by r or \mathcal{R} the radius of a sphere, while R stands for the radius of a circle.

⁷A SIS is a self-gravitating spherical model with *diagonal* pressure tensor and velocity dispersion *independent* of position [27]. We stress that this terminology is somewhat sloppy, since it does *not* mean that the halo velocity dispersion is constant.

B. Satellite galaxies

Beyond the gaseous disk, no stars or cold HI clouds are present. Therefore, tracers of a different kind have to be identified if we are to probe the mass profile of dark halos.

Several bright spirals are surrounded by *satellite* galaxies, considerably less luminous and thus presumably less massive. Therefore, the possibility arises to use these satellite galaxies to probe the behavior of the gravitational field of the corresponding *primary* galaxies. Note that it makes sense to treat both primary and satellite galaxies as point-like objects in first approximation, since their separation is much larger than their size. It goes without saying that the orbital period of these satellites is by far too long to observe a sizeable portion of their orbits, so that it is unavoidable to resort to a *statistical* treatment of the sample of satellite galaxies [30]. The key-assumption which lies at the basis of this method is that all primary galaxies are sufficiently similar to produce in first approximation the *same* effects on their satellites. As a consequence, the so-called *stacking* technique can be applied: *all* N satellite galaxies are supposed to orbit around a *single* primary \mathcal{P} , thereby considerably increasing the statistical relevance of the satellite sample in question $\{\mathcal{S}_\alpha\}$ ($1 \leq \alpha \leq N$).

Actually, denoting by M the mass of \mathcal{P} the simplest approach is to employ a statistical version of the virial theorem, which reads

$$M = \frac{4}{GN} \sum_{\alpha=1}^N v_{r,\alpha}^2 r_\alpha , \quad (3.14)$$

where r_α and $v_{r,\alpha}$ denote the distance and the radial velocity of the α -th satellite galaxy ($1 \leq \alpha \leq N$), respectively, as measured with respect to the primary at an arbitrary time [31].

This method has been applied to a sample of 115 satellites around 69 primaries, having mean luminosity $L_B \simeq 2 \cdot 10^{10} L_{\odot,B}$. Such an analysis entails that dark halos extend beyond $R \simeq 200$ kpc, with $M(200 \text{ kpc}) \simeq 2 \cdot 10^{12} M_\odot$ [32].

Then the corresponding mass-to-light ratio is $\Upsilon_B \simeq 100 \Upsilon_{\odot,B}$. Because this relation can be regarded as *typical* for spiral galaxies, we can state that the mean mass-to-light ratio of these galaxies is

$$\langle \Upsilon_B \rangle_S \simeq 100 \Upsilon_{\odot,B} . \quad (3.15)$$

Recalling the values quoted in Table 3) it follows that *any* spiral obeys the condition

$$M_{\text{dark}} > 30 M_{\text{lum}} , \quad (3.16)$$

thereby implying that all spiral galaxies are totally *dark matter dominated*.

O O O

An analysis of all data available in 1995 for spiral galaxies gives [33]

$$\left\langle \Upsilon_B(r) \right\rangle_S \simeq (60 \pm 10) \left(\frac{r}{0.1 \text{ Mpc}} \right) \Upsilon_{\odot,B} , \quad r < 180 \text{ kpc} . \quad (3.17)$$

3.2 Elliptical galaxies

Stars in elliptical galaxies have a totally different dynamical behavior as compared to stars in spiral galaxies. Indeed, an elliptical galaxy is a totally disordered system, with stars randomly moving in every direction, much in the same way as the molecules of a gas. Nevertheless, an important difference exists with the behavior of a gas. While a gas reaches an equilibrium state through collisions – which ultimately leads to energy equipartition – the stellar population of an elliptical galaxy is collisionless, and the equilibrium state is attained through a process called by the oxymoron of *violent relaxation*. Basically, it is the time-varying gravitational field during galaxy formation that leads to the equipartition of velocity among stars (why velocity instead energy is evident from the fact that mass drops out from the equations of motion, thanks to the equality of inertial and gravitational mass) [34]. Actually, numerical simulations of this process have shown that the resulting surface brightness has the form $I_{\text{lum}} \propto R^{1/4}$, where R is the projected galactocentric distance, which is in very good agreement with observations (see below) [35].

Indeed, luminous matter in elliptical galaxies has a spheroidal distribution, well described by the *De Vaucouleurs* surface brightness profile

$$I(R) \propto \exp \left\{ -7.67 \left[(R/R_e)^{1/4} - 1 \right] \right\}, \quad (3.18)$$

where R_e is the *effective radius* (typically $3 \text{ kpc} < R_e < 10 \text{ kpc}$). In spite of the fact that the stellar motion in ellipticals is highly chaotic – with velocity dispersions usually as large as velocities themselves – another difference with respect to the molecules of a gas exists: due to non-collisionality, the stellar velocity dispersion along the radial direction is generally different from the velocity dispersion along the tangential direction. Manifestly, in such a situation a rotation curve provides *no* information whatsoever about the galactic gravitational field, and so different techniques have to be devised to look for dark matter in elliptical galaxies.

A. Dynamical analysis

A classic approach rests upon the dynamical analysis of stellar motion and can be summarized as follows. Any *specific* stellar population of ellipticals can be thought of as a collisionless fluid in a steady state, resulting from the balance between the kinetic pressure – brought about by the above-mentioned chaotic motion like in a gas – and the overall gravitational field. Assuming spherical symmetry – which is realistic for ellipticals of the Hubble subtypes E0, E1 and E2 – and denoting by r the galactocentric distance, it can be shown that the star number density profile $n_*(r)$ obeys the *Jeans equation* [27]

$$\frac{d}{dr} \left(n_*(r) \sigma_r^2(r) \right) + \frac{2n_*(r)\beta(r)\sigma_r^2(r)}{r} + \frac{GM_{\text{tot}}(r)n_*(r)}{r^2} = 0, \quad (3.19)$$

where $n_*(r)$ is the number density of a given set of stellar tracers while $M_{\text{tot}}(r)$ it the *total* mass of the galaxy responsible for the overall gravitational field. Note that this is just the *Euler equation* for a collisionless fluid with *non-diagonal* pressure tensor and velocity parametrized by the radial dispersion $\sigma_r(r)$ and the anisotropy function $\beta(r)$. It is very easy to see that Eq. (3.19) can be rewritten in the form

$$M_{\text{tot}}(r) = -\frac{\sigma_r^2(r)}{G} \left(\frac{d \ln n_*(r)}{d \ln r} + \frac{d \ln \sigma_r^2(r)}{d \ln r} + 2\beta(r) \right) r. \quad (3.20)$$

So, we can find the overall integrated mass profile $M_{\text{tot}}(r)$ of the elliptical in question provided that we succeed in determining the three functions $n_*(r)$, $\sigma_r(r)$ and $\beta(r)$ from observations. From a conceptual point of view, $M_{\text{tot}}(r)$ plays here the same rôle as $v_c(R)$ did for spiral galaxies: a discrepancy between $M_{\text{tot}}(r)$ and the integrated mass profile of *luminous* matter alone $M_{\text{lum}}(r)$ would quantify the amount of dark matter.

Unfortunately, only the surface brightness profile on the sky $I_*(R)$ and the velocity dispersion profile along the line-of sight $\sigma_{\parallel,*}(R)$ are the commonly available *observables*, and so there is not enough information to uniquely fix the unknown functions $n_*(r)$, $\sigma_r(r)$ and $\beta(r)$ by deprojection. As a result, $M_{\text{tot}}(r)$ can be determined only by making some *Ansatz* on the functional form of $\beta(r)$, such as the *Osipkov-Merritt* one [36, 37]

$$\beta(r) = \frac{r^2}{r^2 + a^2}, \quad (3.21)$$

where a is an arbitrary constant.

For a long time, instrumental limitations prevented the application of such a dynamical analysis to a tracer population having a sufficiently large galactocentric distance, thereby severely hindering its effectiveness. But in the last decade the situation has considerably improved and today globular clusters and planetary nebulae (PNe) allow to map a bright elliptical out to $r \simeq 7R_e$. Moreover, it has become possible to infer $\beta(r)$ by a careful analysis of the galaxy spectral line profiles [38, 39].

As far as dark matter is concerned, the above dynamical analysis leads to a result which *strongly depends* on the galaxy luminosity.

Intermediate ellipticals: As an example of this class, we consider the E1 elliptical NGC 4494 with $R_e = 3.57$ kpc. The line-of-sight velocities of 255 PNe out to $7R_e$ have been measured. It is found that $0.2M_* < M_{\text{dark}} < 0.5M_*$ at $R = R_e$ [40]. Similar results have been obtained for other intermediate ellipticals. Thus, the intermediate ellipticals analyzed so far by PNe as mass tracers are all consistent with $M_{\text{dark}} \simeq 0.4M_*$ inside the optical region.

Bright ellipticals: An enlightening example is provided by the analysis of a set of 21 E0, E1 and E2 ellipticals. It is found that only for three galaxies the existence of dark matter is compelling for $R < 1.5R_e$ even though it is likely to be present in eight of them [41]. A more detailed analysis of the same sample has led to a clarification of the dark matter distribution: some galaxies show no evidence for dark matter inside $2R_e$, while others have $20Y_{B,\odot} < Y_B < 30Y_{\odot,B}$ at $2R_e$. In the latter case – even maximizing the stellar mass – the contribution of dark matter is 10% – 40% at R_e , which means that the condition $M_{\text{dark}} \simeq M_*$ holds true in the range $2R_e < R < 4R_e$ [42].

B. X-ray emission

Bright elliptical galaxies contain ionized gas at temperature $3 \cdot 10^6 \text{ K} < T_{\text{gas}} < 10^7 \text{ K}$, that emits X-rays through the process of ion-recombination and so producing a diffuse luminosity of $10^{38} \text{ ergs}^{-1} < L_X < 10^{42} \text{ ergs}^{-1}$, which has first been detected by the *Einstein* satellite. By using exactly the same method that will be described in detail for regular clusters valuable results have been obtain concerning the dark matter halos surrounding the galaxies in question.

An analysis of all data available in 1995 for elliptical galaxies gives [33]

$$\langle \Upsilon_B(r) \rangle_E \simeq (200 \pm 50) \left(\frac{r}{0.1 \text{ Mpc}} \right) \Upsilon_{\odot, B}, \quad r < 70 \text{ kpc}, \quad (3.22)$$

which holds true for lenticular galaxies as well.

C. Gravitational lensing

A great progress has been made during the last few years in the application of gravitational lensing to elliptical galaxies. As compared to the case of cluster of galaxies the situation is obviously more difficult, because of the much smaller value of the lens mass. Nevertheless, remarkable results have been obtained.

Strong lensing: It can be shown that for a pretty nearby lens we have $\xi_E < R_e$, and so only information about the central galactic region can be obtained. However, when the lens is located at redshift $z > 1$ it turns out that ξ exceeds several R_e , which allows to probe the region where dark matter should dominate. In 2008 a sample of 131 elliptical galaxies with an associated giant arc has been obtained from observations with the Hubble Space Telescope. An analysis of this sample shows that dark matter starts to dominate between $2R_e$ and $3R_e$ [43].

Weak lensing: An alternative strategy for determining the mass of the dark halos exploits the phenomenon of weak lensing. This technique has initially been used in order to discover the presence of dark matter in clusters of galaxies, because – owing to their much larger number of arclets – the polarization can be reliably determined, and so the technique outlined in Section 2.2 (Part B) can be straightforwardly applied. In spite of the great advance in the observational techniques during the last few years, even for massive galaxies the number of arclets around a single elliptical is too small to draw statistically reliable conclusions.

Yet, the so called *galaxy-galaxy lensing* has allowed to sidestep such a difficulty, and so to successfully employ weak lensing even for elliptical galaxies. The way out of the conundrum proceeding as follows. Consider a sample of lenses sufficiently rich and homogeneous made of bright elliptical galaxies. Much in the same way as for the method of satellite galaxies applied to spiral galaxies in Section 3.1 (Part B), the key-assumption here is that all lenses are sufficiently similar to produce in first approximation the *same* effects on the background galaxies close to them in projection. As a consequence, we can again apply the technique of stacking: *all* arclets are attributed to a *single* lens \mathcal{L} , thereby largely increasing the statistical relevance of the arclet sample in question. Several results have been obtained in this way. However, the specific implementation of this approach varies considerably, and so there is no wonder that also some results can be in disagreement among each other. We limit ourselves to quote two of them.

- For non-parametrized lens models with $\Upsilon_{B, \text{lum}} = 3$ the halo mass turns out to be $M_{\text{halo}} = 2 \cdot 10^{12} M_{\odot}$ and $\Upsilon_{B, \text{halo}} \simeq 100 \Upsilon_{\odot}$ [44].
- For parametrized lens model the *total* mass profile can be probed over a typical galactocentric distance $R_e < r < 100 R_e$, and turns out to be isothermal. Moreover, for $\Upsilon_{V, \text{lum}} = 4.5 \Upsilon_{\odot}$ it is found that $\Upsilon_{V, \text{halo}} \simeq 170 \Upsilon_{\odot}$ [45].

3.3 Clusters of galaxies

Galaxies are not randomly distributed throughout the Universe, but tend to aggregate into groups and clusters. As a rough indication, 50% of all galaxies belong to the field, 40% to groups while 10% to clusters. The precise definition of galaxy associations has been provided by Abell in 1958. Broadly speaking, groups contain at most 30 galaxies inside a sphere of the *Abell radius*, conventionally defined as $\mathcal{R}_A \simeq 2.14 \text{ Mpc}$. On the other hand, clusters are made of more than 30 members. For dark matter studies, regular clusters are the most suited ones, since they are the most luminous – encompassing typically more than 500 galaxies – and especially because they are spherically symmetric in first approximation. Their resulting optical luminosity lies in the range $1.2 \cdot 10^{13} L_\odot < L(\mathcal{R}_A) < 1.2 \cdot 10^{14} L_\odot$. While clusters may extend beyond \mathcal{R}_A as gravitationally bound systems, as a rule the region inside \mathcal{R}_A is in equilibrium.

A. Dynamical analysis

Actually, any isolated self-gravitating system reaches an equilibrium state when the age of the system exceeds the time needed by a generic constituent to cross it. This condition is indeed largely met for regular clusters within \mathcal{R}_A . Therefore the validity of the virial theorem in this case is fully justified.

As already pointed out, the first evidence for a large amount of dark matter in the Universe came from the virial analysis of the Coma cluster as carried out by Zwicky in 1933 [7]. This strategy has since been applied to many regular clusters and it is enlightening to repeat Zwicky's exercise in somewhat general term.

Let us apply the virial theorem to the cluster galaxies – assuming that they are the only matter component – according to which the average potential energy U is related to the average kinetic energy K by

$$2K + U = 0. \quad (3.23)$$

Assuming spherical symmetry, the potential energy can be represented as

$$U = -\frac{\alpha GM_A^2}{\mathcal{R}_A}, \quad (3.24)$$

where M_A is the total cluster mass in galaxies inside \mathcal{R}_A and α is a constant which reflects the actual density profile of cluster galaxies. Because we can only measure the global line-of-sight velocity dispersion σ_{\parallel} , we have to assume global isotropy in velocity space, so that we have

$$K = \frac{1}{2}M\langle v^2 \rangle = \frac{3}{2}M\sigma_{\parallel}^2. \quad (3.25)$$

Whence

$$M = \frac{\mathcal{R}_A \sigma_{\parallel}^2}{G} \simeq 5 \cdot 10^{14} \left(\frac{\sigma_{\parallel}}{1000 \text{ Kms}^{-1}} \right)^2 M_\odot, \quad (3.26)$$

since the observed galaxy density profile leads to the choice $\alpha = 3$. Because for regular clusters the median value of σ_{\parallel} is $\sigma_{\parallel} \simeq 750 \text{ Kms}^{-1}$ and the median number of galaxies is 500, we ultimately get $M \simeq 5.6 \cdot 10^{11} M_\odot$. Recalling for comparison that the luminous mass of the Milky Way is

$M_{\text{MW,lum}} \simeq 5.4 \cdot 10^{10} M_{\odot}$, we conclude that 90% of the mass in each cluster galaxy is missing on average. A more sophisticated analysis shows that the missing mass is even larger [46].

A sample of values of the mass-to-light ratio Υ_{RC} for regular clusters derived by the virial theorem is reported in Table 3 [47].

Table 4

Cluster	$\Upsilon_{RC}/\Upsilon_{\odot,RC}$
A2390	173
MS0016 + 16	202
MS0302 + 16	157
MS0440 + 02	218
MS0451 + 02	250
MS0451 – 3	275
MS0839 + 29	200
MS0906 + 11	560
MS1006 + 12	204
MS1008 – 12	154
MS1224 + 20	148
MS1231 + 15	123
MS1358 + 62	138
MS1455 + 22	412
MS1512 + 36	164
MS1621 + 26	106

B. X-ray emission

Regular clusters of galaxies contain a large amount of hot ionized gas at a temperature $1 \cdot 10^7 \text{ K} < T_{\text{gas}} < 1.5 \cdot 10^8 \text{ K}$ – whose mass exceeds the luminous mass in galaxies – that produces a diffuse X-ray emission with luminosity $6 \cdot 10^{42} < L_X < 2 \cdot 10^{45} \text{ erg s}^{-1}$ which has first been detected by the *Uhuru* satellite. The situation is analogous to what happens in elliptical galaxies, apart from the fact that the higher temperature makes thermal Bremsstrahlung the dominant process [48].

It has soon been recognized that such an X-ray emission can be used to estimate the total cluster mass where the gas is present under the following assumptions.

- The gas should be spherically distributed and gravitationally bound to the cluster.
- The gas can be treated as an optically thin, weakly collisional perfect fluid in ionization and local thermodynamic equilibrium.
- The gas has to be in hydrostatic equilibrium in the overall gravitational potential

Let us schematically outline the logic of the argument. For simplicity, we suppose that $T_{\text{gas}} =$ constant.

Step 1: An excellent fit to the data is provided by the so-called β -profile as an *Ansatz* for $I_X(R)$

$$I_X(R) = I_{X,0} \left[1 + \left(\frac{R}{a_X} \right)^2 \right]^{-3\beta+1/2}, \quad (3.27)$$

which determines the free parameters $I_{X,0}$, a_X and β . As an orientation, according to the observations performed with the last generation of X-ray observatories it is typically found $150 \text{ kpc} < a_X < 200 \text{ kpc}$ and $0.4 < \beta < 1.0$, with median values $a_X \simeq 150 \text{ kpc}$ and $\beta \simeq 0.67$. More accurate but also more complicated parametrizations can be employed, but the logic remains unchanged.

Step 2: We deproject $I_X(R)$ thereby finding the volume emissivity

$$\mathcal{E}_X^{\text{tb}}(r) \propto \left[1 + \left(\frac{r}{a_X} \right)^2 \right]^{-3\beta}. \quad (3.28)$$

Step 3: Recalling that in the present case the volume emissivity is

$$\mathcal{E}_X^{\text{tb}}(r) = n_{\text{gas}}^2(r) \Lambda_{\text{tb}}(T) \propto n_{\text{gas}}^2 \left(\frac{T_{\text{gas}}}{10^8 \text{ K}} \right)^{1/2} \text{ erg cm}^3 \text{ s}^{-1}, \quad (3.29)$$

we obtain

$$n_{\text{gas}}(r) \propto \left[1 + \left(\frac{r}{a_X} \right)^2 \right]^{-3\beta/2}. \quad (3.30)$$

Step 4: By combining the conditions of hydrostatic equilibrium, local thermodynamic equilibrium and $T_{\text{gas}} = \text{constant}$, it is a simple exercise to recast the usual equation $dP(r)/dr = -G\rho(r)M_{\text{tot}}(r)/r^2$ into the form

$$M_{\text{tot}}(r) = -\frac{k_B T_{\text{gas}}}{G\mu m_p} \frac{d \ln n_{\text{gas}}(r)}{d \ln r} r, \quad (3.31)$$

where $\mu \simeq 0.6$ denotes the mean molecular weight for a fully ionized gas with solar composition.

Step 5: By inserting Eq. (3.30) into Eq. (3.31) we finally get

$$M_{\text{tot}}(r) = \frac{3\beta k_B T_{\text{gas}}}{G\mu m_p} \frac{(r/a_X)^2}{1 + (r/a_X)^2} r, \quad (3.32)$$

Now, in order to bring out the physical meaning of Eq. (3.32) we take typical values for the relevant parameters: $a_X = 175 \text{ kpc}$, $\beta = 0.67$ and $T_{\text{gas}} = 10^8 \text{ K}$. Since modern models of structure formation predict that also regular clusters are surrounded by a dark matter halo, we want to use Eq. (3.32) to figure out its integrated mass profile. So, we work in the approximation $r > a_X$. As a consequence, we see that in this region the halo has an isothermal profile. Moreover, we find from Eq. (3.32) for our benchmark values of the parameters

$$M_{\text{tot}}(r) \simeq 6.49 \cdot 10^{14} \left(\frac{r}{\text{Mpc}} \right) M_{\odot}. \quad (3.33)$$

While the gas is obviously a constituent of the cluster halo, a nontrivial contribution from dark matter is present. Indeed, we know that dark matter dominates galaxies, and so it necessarily lurks

inside regular clusters. Moreover, some further dark matter can exist in the intracluster space. So, the real question is whether hot gas or dark matter dominates the cluster mass budget. It goes without saying that this issue can be resolved by evaluating the gas mass fraction

$$f_g(r) \equiv \frac{M_g(r)}{M(r)} \quad (3.34)$$

for the above benchmark values of the parameters. Under our assumptions it turns out that f_g is *independent* of r (this is simply due to $\beta \simeq 0.7$) and we get

$$f_g \simeq 0.12 . \quad (3.35)$$

In addition, the total gas mass comes out invariably *larger* than the luminous mass of the cluster galaxies. Thus, we conclude that also regular clusters of galaxies are dominated by *dark matter* [49, 50, 51].

C. Gravitational lensing

Strong lensing: The application of strong gravitational lensing is straightforward, and we have nothing to add to the discussion presented in Section 2.2 (Part A). A wonderful picture of an almost perfect Einstein ring in the image of a lensing cluster is shown in Figure 4.

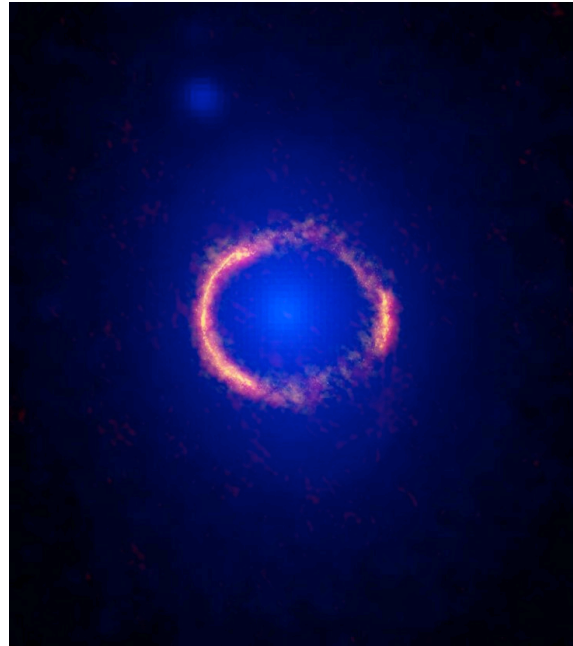


Figure 3: Giant arcs in the image of sdp81-alma

Weak lensing: As already anticipated, the application of weak lensing to regular clusters is straightforward due to the presence of the so-called *Tyson population* of background faint blue galaxies with a surprisingly high surface number density, so that the arcllet polarization can be easily determined (at least in principle) [14].

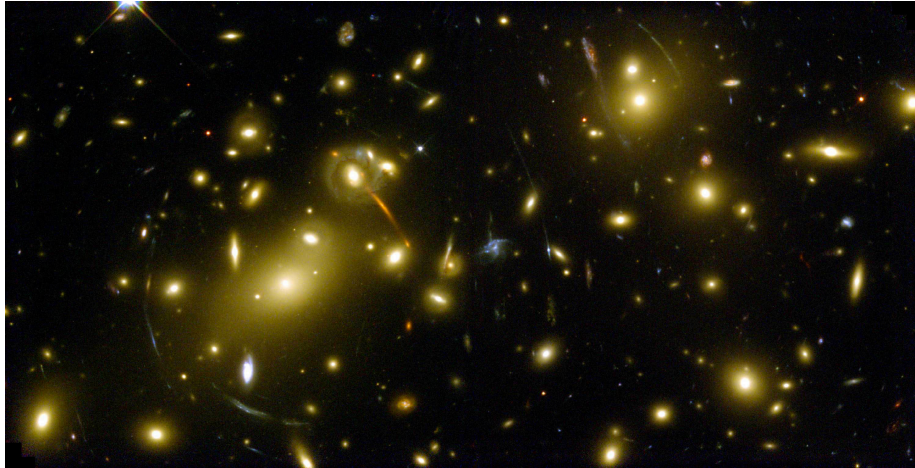


Figure 4: Arclets in the image of Abell 2218

We stress that – at variance with the previous methods – the mass determination based on gravitational lensing does *not* require any assumption about the dynamical state of the cluster. It is gratifying that even this strategy yields values of the mass-to-light ratio which generally *agree* with those derived by the virial analysis and X-ray studies.

Specifically, the application of the above-discussed techniques to *regular* clusters gives values lying around the mean

$$\langle \Upsilon_B \rangle_{\text{RC}} \simeq 210 \Upsilon_{\odot, B}. \quad (3.36)$$

Because regular clusters contain mostly lenticular and elliptical galaxies and only a small fraction of spirals, Eq. (3.36) is in very good agreement with Eqs. (3.17) and (3.22).

Clusters obviously contain the dark matter present in the cluster galaxies, but it might well happen that *additional* dark matter lurks in the intracluster space. However, an explicit analysis shows that the *total* galactic matter plus the hot gas *fully* account for the *total* cluster mass, thereby ruling out such a possibility [33].

4. A glimpse to cosmology

The hot big bang cosmological model describes an *idealized* Universe made of a smooth mass distribution. Such a smeared-out mass distribution forms a fluid called the *cosmic substratum* (CS) by Weyl, which is a self-gravitating system described by general relativity. So – denoting by $g_{\mu\nu}(x)$ the metric of the CS – its constituents move along the corresponding time-like geodesics.

The conceptual basis of the hot big bang cosmological model is the *Weyl principle* stated in 1923, according to which the geodesics of the CS form a *normal congruence* of time-like world-lines with the exception of a point in the past and possibly a point in the future [52]. The Weyl principle surprisingly predates the Hubble’s discovery in 1929 of the expansion of the Universe [53] and has several far-reaching consequences.

- The observers $\{\mathcal{O}_{\mathcal{F}}\}$ co-moving with the CS form a set of preferred observers, who are on the same footing as far as the description of the Universe is concerned.
- The time-like geodesics of any $\{\mathcal{O}_{\mathcal{F}}\}$ can be represented as $x^i = \text{constant}$ ($1 \leq i \leq 3$).
- The three-dimensional hyper-surfaces anywhere normal to the time-like geodesics in question can be represented as $x^0 = \text{constant}$.
- Each $\{\mathcal{O}_{\mathcal{F}}\}$ can use the four-dimensional coordinate system $\{x^\mu\}$ ($0 \leq \mu \leq 3$). Moreover, the metric of all $\{\mathcal{O}_{\mathcal{F}}\}$ lacks terms mixing x^0 and $\{x^i\}$ ($1 \leq i \leq 3$).
- Since all $\{\mathcal{O}_{\mathcal{F}}\}$ are free-falling in the gravitational field produced by the CS, each measures his/her proper time, which turns out to be the *same* for all of them. Therefore, there exists a *universal* cosmic time t which is just the proper time measured by a generic $\{\mathcal{O}_{\mathcal{F}}\}$.
- At any value of t the *cosmological principle* holds true for any $\{\mathcal{O}_{\mathcal{F}}\}$, who therefore sees that the Universe is *homogeneous* and *isotropic*. As a consequence, the three-dimensional space has *constant* curvature.

Because homogeneity holds true at any time, it turns out that the most general metric of the CS as seen by a generic $\{\mathcal{O}_{\mathcal{F}}\}$ has the Robertson-Walker form

$$ds^2 = c^2 dt^2 - R^2(t) \left[\frac{dr^2}{1 - kr^2} + r^2 (d\theta^2 + \sin^2 \theta d\phi^2) \right], \quad (4.1)$$

where $R(t)$ is the cosmic scale factor and the constant k is proportional to the gaussian curvature of tridimensional space. Then we have

$$\text{Tridimensional space is } \begin{cases} \text{OPEN or HYPERBOLIC for } k < 0, \\ \text{FLAT or EUCLIDEAN for } k = 0, \\ \text{CLOSED or SPHERICAL for } k > 0. \end{cases} \quad (4.2)$$

Thus, the only possible fate of the Universe is a *global* expansion or contraction. We assume henceforth that the Universe *expands*, in accordance with observations. We also denote by t_0 the present time. Another implication of the cosmological principle is that the CS is a *perfect* fluid described by the energy-momentum tensor $T^{\mu\nu}(t)$ containing the energy density $\rho(t)c^2$ and the pressure $P(t)$ of the CS (they do not depend on \mathbf{x} because of space homogeneity). The co-moving coordinates are taken to be dimensionless, and it is evident that all lengths scale proportionally to $R(t)$. In particular, this is true for the wavelength λ of photons, so that we have $\lambda(t) \propto R(t)$. Let us consider a photon emitted at time $t < t_0$ with wavelength $\lambda(t)$ and detected at present with wavelength $\lambda(t_0)$. As in the Doppler effect, it is very useful to define the *redshift*

$$z \equiv \frac{\lambda(t_0) - \lambda}{\lambda}, \quad (4.3)$$

which – owing to $\lambda(t) \propto R(t)$ – becomes

$$z = \frac{R(t_0) - R(t)}{R(t)} = \frac{R(t_0)}{R(t)} - 1. \quad (4.4)$$

Hence, we see that as long as $R(t)$ is a monotonic function of t the redshift is a very suitable parameter to describe the evolution of the Universe: during the *expansion* we have $R(t) < R(t_0)$, which implies that $R(t)$ increases with t and λ increases as well, thereby entailing that the radiation we receive is shifted towards *larger wavelengths*. However, the interpretation is different from that of the Doppler effect: here the redshift is not due to the receding motion of a source with respect to us, but rather to the expansion of tridimensional space.

The dynamics of the Universe is parametrized by the cosmic scale factor, which obeys the equations arising upon insertion of the metric $g_{\mu\nu}(x)$ as dictated by Eq. (4.1) and $T^{\mu\nu}(t)$ into Einstein field equations. This step is deceptively simple. Einstein field equations hold true in the real world, but here we are concerned with the idealized world made of the CS, where matter is smoothed out. Whatever smoothing process is adopted, the Einstein field equations with a smoothed energy-momentum tensor *cannot* yield the smoothed metric of the CS simply because they are highly non-linear. As a consequence, the so-called *back-reaction* shows up [54, 55], which is unfortunately generally ignored. Hence we get the Friedmann equations

$$\left(\frac{\dot{R}(t)}{R(t)}\right)^2 = \frac{8\pi G}{3}\rho(t) - \frac{kc^2}{R^2}, \quad (4.5)$$

$$\frac{\ddot{R}(t)}{R(t)} = -\frac{4\pi G}{3}\left(\rho(t) + \frac{3P(t)}{c^2}\right), \quad (4.6)$$

which describe our idealized Universe (provided that the back-reaction is negligible). Observe that by combining Eqs. (4.5) and (4.6), the following conservation equation arises

$$\frac{d}{dt}(\rho R^3(t)) = -\frac{3P(t)}{c^2}R^2(t)\dot{R}(t). \quad (4.7)$$

What remains to be specified at this point is the equation of state of the cosmic substratum, namely the relationship between $\rho(t)$ and $P(t)$. It is useful to write such a relation in the form

$$P(t) = w\rho(t)c^2, \quad (4.8)$$

where w – which can be supposed *constant* – takes the values 0 for non-relativistic *matter*, $1/3$ for *radiation* and -1 in the presence of a nonvanishing vacuum energy, usually described by the *cosmological constant*. Note that in the latter case, $\rho(t)$ and $P(t)$ have *opposite* signs, and so whenever $\rho(t) + 3P(t)/c^2$ is positive the r.h.s. of Eq. (4.7) is negative and the expansion is *decelerated*, whereas in the opposite case the expansion is *accelerated*. Finally, by inserting Eq. (4.8) into Eq. (4.7), we get

$$\rho(t) \propto R^{-3(1+w)}(t), \quad (4.9)$$

thereby implying that $\rho \propto R^{-3}(t)$ for nonrelativistic matter, $\rho \propto R^{-4}(t)$ for radiation and $\rho = \text{constant}$ for a cosmological constant.

Now, it is very convenient to define the following parameters, where the suffix 0 denote the present value, namely at time t_0 .

Hubble parameter:

$$H(t) \equiv \frac{\dot{R}(t)}{R(t)}, \quad H_0 \simeq 70 \text{ Kms}^{-1} \text{ Mpc}^{-1}, \quad (4.10)$$

which entails that the Universe *expands* for $H(t) > 0$ and *contracts* for $H(t) < 0$.

Hubble time:

$$t_H(t) \equiv \frac{1}{H(t)}, \quad t_{H,0} \simeq 13.97 \text{ Gyr}. \quad (4.11)$$

Hubble radius:

$$d_H(t) \equiv \frac{c}{H(t)}, \quad d_{H,0} \simeq 4.29 \text{ Gpc}. \quad (4.12)$$

Critical density:

$$\rho_{\text{cr}}(t) \equiv \frac{3H^2(t)}{8\pi G}, \quad \rho_{\text{cr},0} \simeq 9.21 \cdot 10^{-30} \text{ g cm}^{-3}. \quad (4.13)$$

Cosmic density parameter:

$$\Omega(t) \equiv \frac{\rho(t)}{\rho_{\text{cr}}(t)}, \quad \Omega_0 = ?. \quad (4.14)$$

It is also very useful to define for each component of the CS a cosmic density parameter $\Omega_M(t)$, $\Omega_R(t)$ and Ω_Λ which add up to $\Omega(t)$. Moreover, we shall see that it proves very convenient to similarly define $\Omega_{\text{LUM}}(t)$ for the *luminous* matter, $\Omega_{\text{GAL}}(t)$ for the whole matter in galaxies and $\Omega_B(t)$ for the total *ordinary* matter, conventionally referred to as baryons (even is it includes leptons). Now, Eqs. (4.10), (4.13) and (4.14) allow us to rewrite the Friedmann Eq. (4.5) as

$$\Omega(t) = 1 + \frac{kc^2}{H^2(t)R^2(t)}. \quad (4.15)$$

which implies that

$$\text{Tridimensional space is } \begin{cases} \text{OPEN or HYPERBOLIC for } \Omega(t) < 1, \\ \text{FLAT or EUCLIDEAN for } \Omega(t) = 1, \\ \text{CLOSED or SPHERICAL for } \Omega(t) > 1. \end{cases} \quad (4.16)$$

Deceleration parameter:

$$q(t) \equiv -\frac{R(t)\ddot{R}(t)}{\dot{R}^2(t)} = \frac{1}{2} \left(\Omega_M(t) + 2\Omega_R(t) - 2\Omega_\Lambda \right). \quad (4.17)$$

Therefore, by assuming that the Universe is expanding at time t , it follows that the expansion is *decelerated* for $2\Omega_\Lambda < \Omega_M(t) + 2\Omega_R(t)$ whereas it is *accelerated* for $2\Omega_\Lambda > \Omega_M(t) + 2\Omega_R(t)$.

Observe that no transition among the three possibilities in Eq. (4.16) is allowed.

O O O

The foregoing discussion has shown that the knowledge of the various cosmic density parameters is crucial for cosmology.

- According to Eq. (4.15), the actual value of $\Omega(t)$ tells us about the geometry of tridimensional space.

- Moreover, the relative values of $\Omega_M(t)$, $\Omega_M(t)$ and Ω_Λ establish whether the expansion is decelerated or accelerated.

Before proceeding further, we stress that all cosmological density parameters to be quoted below refer to the present Universe, and for notational simplicity the subindex 0 will be dropped.

Therefore, the rest of this proceeding is devoted to the *observational determination* of the present values of the various cosmic density parameters.

5. Cosmological relevance of the astrophysical analysis

What does the astrophysical analysis tell us about such a crucial issue?

To this end, we have to consider the *galaxy luminosity function* $\varphi(L)$, which yields the average number density of galaxies per unit volume and per unit luminosity. As a consequence, the average luminosity density of all galaxies \mathcal{L} reads

$$\mathcal{L} = \int_0^\infty dL L \varphi(L). \quad (5.1)$$

The best-fit analytic expression for $\varphi(L)$ is the one proposed in 1976 by Schechter [56]. It has become known as the *Schechter luminosity function* and is written in the conventional form

$$\varphi(L) = \frac{\varphi^*}{L^*} \left(\frac{L}{L^*} \right)^\alpha e^{-L/L^*}, \quad (5.2)$$

where L^* , φ^* and α are free parameters to be determined by observations. Accordingly, Eq. (5.1) becomes

$$\mathcal{L} = \int_0^\infty dL L \varphi(L) = \varphi^* L^* \Gamma(\alpha + 2), \quad (5.3)$$

where $\Gamma(\cdot)$ is the Euler gamma function. What Schechter discovered is that this expression for $\varphi(L)$ is accurate for field galaxies, but in first approximation it applies to galaxies in groups and clusters as well.

As a matter of fact, a crucial circumstance is that the *whole* optical luminosity of the Universe is produced by galaxies (this is not the case for instance in the microwave band). Now, the concept of mass-to-light ratio can be appreciated, since it is a very simple device to turn the luminosity of a galaxy into its mass density. As an application, we estimate Ω_{LUM} following Fukugita, Hogan and Peebles (FHP) [57]. In spite of the fact that today the observed values of \mathcal{L}_Y are known with the limitation that ellipticals are not distinguished from lenticulars and that the value for irregulars is unknown [58], the forthcoming analysis relies only on the total luminosity density \mathcal{L}_B as given by Eq. (5.3) with $L_B^* = 1.96 \cdot 10^{10} L_{\odot,B}$, $\varphi^* = 5.52 \cdot 10^{-3} \text{Mpc}^{-3}$, $\alpha = -1.21$, leading to $\mathcal{L}_B = 1.27 \cdot 10^8 L_{\odot,B} \text{Mpc}^{-3}$ as determined by the 2dF (2 degree field survey) [59], in good agreement with the one derived by the SDSS (Sloan digital sky survey) [60].

As a first step, the whole galaxy population is divided into bulges, disks and irregular galaxies. Accordingly, one has to infer the average luminosity density contributed by each of them, namely $\mathcal{L}_{\text{Bulge},B}$, $\mathcal{L}_{\text{Disk},B}$ and $\mathcal{L}_{\text{Irr},B}$. Next, they can be translated into the corresponding average luminous

mass densities ρ_{Bulge} , ρ_{Disk} and ρ_{Irr} upon multiplication by the $\langle \Upsilon_{*,B} \rangle_{\text{Bulge}}$, $\langle \Upsilon_{*,B} \rangle_{\text{Disk}}$ and $\langle \Upsilon_{*,B} \rangle_{\text{Irr}}$, respectively, which are given in Table 3.

We proceed by expressing $\mathcal{L}_{\text{Bulge},B}$, $\mathcal{L}_{\text{Disk},B}$ and $\mathcal{L}_{\text{Irr},B}$ in terms of two previously defined quantities: the B -band bulge luminosity fraction $\mathcal{B}_{Y,B}$ and the mean fractional luminosity density \mathcal{F}_Y contributed by all galaxies of the Hubble type Y . Whence

$$\mathcal{L}_{\text{Bulge},B} = \mathcal{L}_B \sum_Y \mathcal{B}_{Y,B} \mathcal{F}_Y, \quad \mathcal{L}_{\text{Disk},B} = \mathcal{L}_B \sum_Y (1 - \mathcal{B}_{Y,B}) \mathcal{F}_Y, \quad \mathcal{L}_{\text{Irr},B} = \mathcal{L}_B \mathcal{F}_{\text{Irr}}, \quad (5.4)$$

where in the sum the irregulars should be excluded. The values of $\mathcal{B}_{Y,B}$ are taken from Table 2. Previous studies [61, 62] give the values of \mathcal{F}_Y , which are reported in Table 5.

Table 5

Y	\mathcal{F}_Y
E	0.11
S0	0.21
Sa	0.28
Sb	0.29
Sc	0.045
Irr	0.061

Accordingly, Eqs. (5.4) yields

$$\mathcal{L}_{\text{Bulge},B} = 0.385 \mathcal{L}_B, \quad \mathcal{L}_{\text{Disk},B} = 0.556 \mathcal{L}_B, \quad \mathcal{L}_{\text{Irr},B} = 0.061 \mathcal{L}_B, \quad (5.5)$$

and so it follows that the average luminous mass density of *all* galaxies ρ_{LUM} reads

$$\rho_{\text{LUM}} = \langle \Upsilon_{*,B} \rangle_{\text{Bulge}} \mathcal{L}_{\text{Bulge},B} + \langle \Upsilon_{*,B} \rangle_{\text{Disk}} \mathcal{L}_{\text{Disk},B} + \langle \Upsilon_{*,B} \rangle_{\text{Irr}} \mathcal{L}_{\text{Irr},B}. \quad (5.6)$$

Finally, by inserting the values reported in Table 3, adopting the value of \mathcal{L}_B quoted above and dividing by $\rho_{\text{cr},0}$ we get

$$\Omega_{\text{LUM}} = 0.0035. \quad (5.7)$$

This is a fundamental result, because it tells us the value of the cosmic density parameter if only luminous matter were present.

O O O

Because regular clusters are so extended and practically nothing escapes from them during their evolution, it seems natural to suppose that they just reflect the mean composition of the whole Universe [63]. As a consequence, the *cluster* baryon fraction f_B should equal the *cosmic* baryon fraction, and so we get

$$f_B = \frac{\Omega_B}{\Omega_M}. \quad (5.8)$$

According to the result of the satellite PLANCK we have $f_B = 0.144$ [64]. Therefore Eq. (5.8) yields

$$\Omega_M = 6.94 \Omega_B. \quad (5.9)$$

6. Cosmological approach

Cosmological observations not only provide additional and dramatic evidence for the existence of a large amount of dark matter in the Universe, but they also offer fundamental information about its physical nature.

6.1 Primordial nucleosynthesis

A crucial implication of the hot big bang cosmological model is that light elements – like deuterium D, helium He^3 , He^4 and lithium Li^7 – must have formed during the first few minutes of the life of the Universe. Incidentally, we know that the overwhelming majority of the elements are produced in stellar nucleosynthesis, but in order for its prediction to agree with observations the original material forming the first stars should contain about 75 % of hydrogen, 25 % of He^4 with some traces of D and Li^7 .

Because the temperature monotonically decreases during the cosmic expansion, atomic nuclei can form when the energy of background photons becomes lower than the nuclear binding energy. With the number of light neutrinos fixed to 3, the predicted light element abundances depend on a single free parameter, the cosmic baryon density Ω_B . In fact, calculations show that an increase of Ω_B leads to slightly more He^4 , but the resulting amounts of D and He^3 drop dramatically. So, a comparison between the predicted and observed light element abundances unambiguously fixes Ω_B [65]. Indeed, the agreement is achieved for Ω_B within a narrow range

$$0.04 \leq \Omega_B \leq 0.05 . \quad (6.1)$$

In Figure 5 the abundances of light elements as predicted by the big bang nucleosynthesis are plotted versus the baryon-to-photon ratio η , which can be shown to be related to Ω_B by

$$\Omega_B = 7.47 \cdot 10^7 \eta . \quad (6.2)$$

Also the observed light element abundances are indicated by boxes. The narrow vertical band indicates the CMB measure of the cosmic baryon density (three-year WMAP data), while the wider band indicates the big bang nucleosynthesis concordance range (both at 95 % CL).

A remark is in order. No astrophysical process is known in which D is produced, and so all deuterium present in the Universe should be cosmological. Consequently, the comparison between theory and observation is particularly clean in this case. In addition, local estimates of D abundance are in good agreement with measurements in high-redshift clouds along the line of sight to a distant quasar.

Regardless of big bang nucleosynthesis, an *independent* estimate of Ω_B – which turns out to agree with Eq. (6.1) – arises from the features of high-redshift Lyman- α forest absorption lines of neutral hydrogen observed in the spectra of background quasars [66].

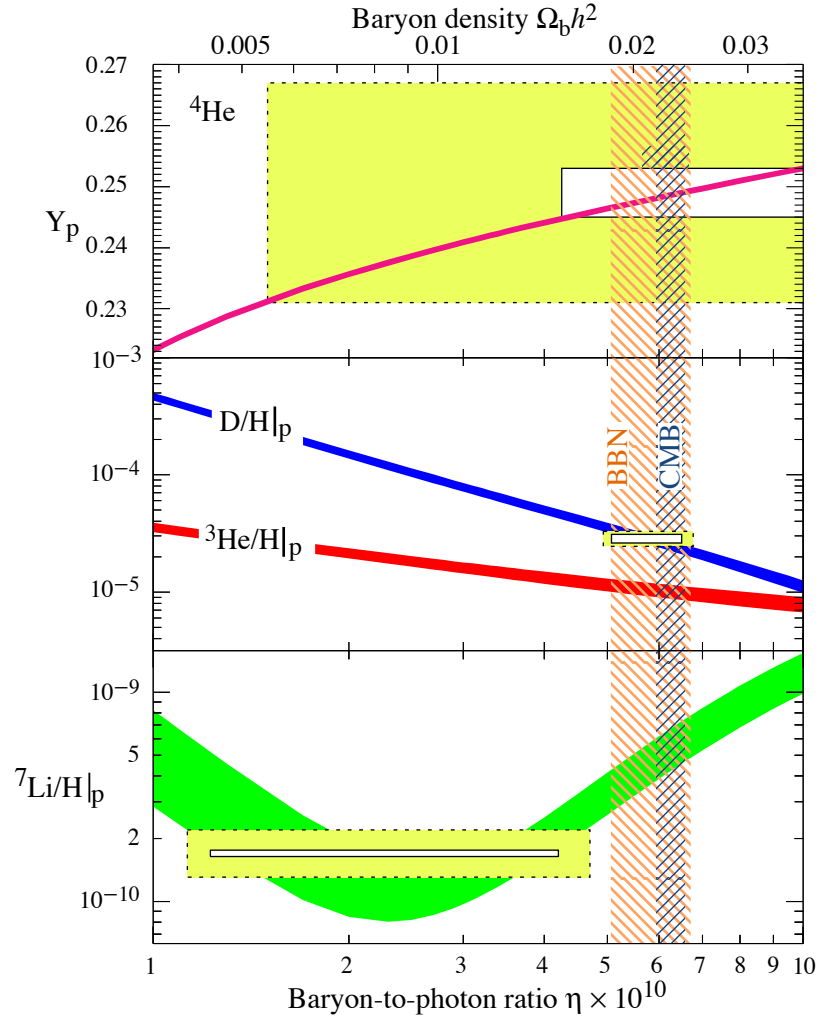


Figure 5: The abundances of D, He³, He⁴ and Li⁷ as predicted by the big bang nucleosynthesis. The bands represent the 95% CL range. Boxes indicate the observed light element abundances (smaller boxes: $\pm 2\sigma$ statistical errors; larger boxes: $\pm 2\sigma$ statistical and systematic errors). The narrow vertical band indicates the CMB measure of the cosmic baryon density (three-year WMAP data), while the wider band indicates the big bang nucleosynthesis concordance range (both at 95% CL).

Before turning to a different argument, an important point should be stressed. Combining Eqs. (5.9) and (6.1), we find

$$0.28 < \Omega_M < 0.35 . \quad (6.3)$$

This simple argument shows that a Universe made of matter alone is necessarily open (hyperbolic) and the expansion is necessarily decelerated. Since matter attract itself, such a conclusion seems obvious.

6.2 Cosmic Microwave Background

The existence of the Cosmic Microwave Background (CMB) is not only a wonderful confir-

mation of the hot big bang cosmological model, but also provides a wealth of information about the early Universe [67, 68, 70, 69].

As we have seen, about a few minutes after the big bang light nuclei form, when the temperature falls below the nuclear binding energy. At this epoch the Universe is made of an optically thick plasma: the photon mean free path is very small and photons are in thermodynamic equilibrium with matter. Hence, they have a blackbody spectrum. After about 380.000 years since the big bang, the temperature drops to such a value that stable atoms can form, a process currently referred to as *recombination* (even though electrons and nuclei had never combined before). This process takes place at $z_{\text{rec}} \simeq 1100$, corresponding to $t_{\text{rec}} \simeq 3 \cdot 10^5$ years after the big bang. As a consequence, matter becomes neutral and decouples from radiation, so that the Universe now becomes transparent to photons. They can travel unimpeded, thereby carrying us a snapshot of the Universe when it was only 380.000 years old. Moreover, it is easy to show that blackbody spectrum is preserved during the expansion: only its temperature decreases as $T_{\text{cmb}}(t) \propto R^{-1}(t)$. Today the peak temperature of the CMB is $T_{\text{cmb}}(t) = 2.725$ K.

Early analyses showed that the CMB is highly isotropic, once our peculiar motion – producing the *dipole anisotropy* with $\Delta T/T_0 \sim 10^{-3}$ – is corrected for. However, in 1992 the COBE mission discovered intrinsic *anisotropies* in the CMB spectrum, corresponding to temperature *fluctuations* $\Delta T/T_0 \sim 10^{-5}$ on the angular scale of 7° . Remarkable progress has been made in the subsequent years, with the BOOMERANG [71], MAXIMA [72] and DASI [73] missions detecting similar temperature fluctuations down to 1° . More recently, the WMAP mission has succeeded in discovering temperature fluctuations on the angular scale of 0.2° [74], which are confirmed by the presently operating PLANCK mission.

What is the physical meaning of the CMB fluctuations? Because the post-recombination Universe is essentially transparent to the CMB photons, those which we detect now had their last interaction with matter on a virtual sphere – centered at our position – named *last scattering surface* (LSS). At the time of recombination, a generic point of the LSS had an horizon of radius $\mathcal{R}_{\text{rec}} = 3ct_{\text{rec}}$ (since the Universe is matter dominated), which we see today under an angle θ_1 . Therefore, only events lying within θ_1 – about a given direction in the sky – were causally connected at recombination. As a consequence, only CMB fluctuations on angular scales $\theta < \theta_1$ yield information about physical processes occurring during recombination. However, recombination was not an instantaneous process, and this fact implies that the LSS is a shell of *finite* thickness, corresponding to an observed angular scale θ_2 (obviously $\theta_2 < \theta_1$). As a result, CMB fluctuations get smeared out over angular scales $\theta < \theta_2$. Thus, we conclude that recombination physics shows up in CMB fluctuations on angular scales in the range $\theta_2 < \theta < \theta_1$. These fluctuations are the imprint on the CMB of *baryon acoustic oscillations* in the matter-radiation fluid just before decoupling, with gravity providing the driving force while radiation pressure causes the restoring one [75].

A quantitative description of the CMB fluctuations emerges from a statistical treatment based on the harmonic analysis of $\Delta T/T_0$. Were measurements be performed on a plane, $\Delta T/T_0$ would depend on x, y and we would represent $\Delta T/T_0(x, y)$ as a Fourier series. However, $\Delta T/T_0$ is measured on the celestial sphere and so it depends on θ, φ . Accordingly, the following multipole expansion

naturally arises

$$\frac{\Delta T}{T_0}(\theta, \varphi) = \sum_{l=0}^{\infty} \sum_{m=-l}^l a_{lm} Y_{lm}(\theta, \varphi), \quad (6.4)$$

where $Y_{lm}(\theta, \varphi)$ are spherical harmonics and the coefficients a_{lm} are *gaussian random variables* defined by

$$\langle a_{lm} \rangle = 0, \quad (6.5)$$

$$\langle a_{lm} a_{l'm'}^* \rangle = c_l \delta_{ll'} \delta_{mm'}, \quad (6.6)$$

with $\langle \dots \rangle$ representing the average over the whole sky. Denoting by α the angle between two arbitrary directions $\hat{n} \equiv (\theta, \varphi)$ and $\hat{n}' \equiv (\theta', \varphi')$ ($\cos \alpha = \hat{n} \cdot \hat{n}'$), the CMB *autocorrelation function* is

$$C(\alpha) \equiv \left\langle \frac{\Delta T}{T}(\theta, \varphi) \frac{\Delta T}{T}(\theta', \varphi') \right\rangle. \quad (6.7)$$

It can be shown that the autocorrelation function is represented in terms of the *multipole moments* c_l as

$$C(\alpha) = \frac{1}{4\pi} \sum_{l=0}^{\infty} (2l+1) c_l P_l(\cos \theta), \quad (6.8)$$

where $P_l(\cos \theta)$ are Legendre polynomials. It turns out that each term in Eq. (6.8) corresponds to a well-defined angular scale, given by

$$\theta \simeq \frac{180^\circ}{l}. \quad (6.9)$$

Hence, fluctuations on *small* angular scales correspond to *large* multipole orders and vice-versa. Consider now the CMB *power spectrum*, namely the plot of $l(l+1)c_l$ versus l , and denote by l_1 and l_2 the multipole orders corresponding – through Eq. (6.9) – to θ_1 and θ_2 , respectively. Then the baryon acoustic oscillations show up as *acoustic peaks* in the CMB power spectrum within the interval $l_1 < l < l_2$. It is precisely these peaks that tell us much about dark matter.

Specifically, the situation can be summarized as follows. It would be impossible to derive the results presented below in an analytic fashion, and the standard derivation is accomplished with the computer package CMBFAST [76].

- The *position* of the first peak is controlled by θ_1 . Being an angle, θ_1 is very sensitive to the geometry of the Universe, that is to say to Ω . So, the actual position of the first peak yields the specific value of Ω . The result of the PLANCK collaboration is [77]

$$\Omega = 1 \pm 0.012. \quad (6.10)$$

- The *ratio* of the *heights* of the first to the second peak gives Ω_B , whose value reported by the PLANCK collaboration is [77]

$$\Omega_B = 0.049 \pm 0.92. \quad (6.11)$$

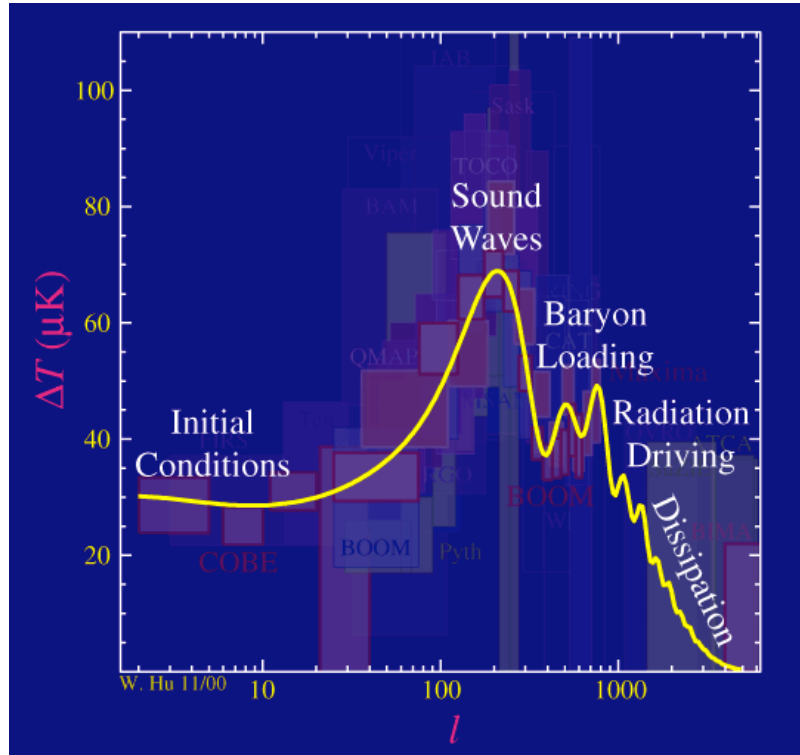


Figure 6: Acoustic peaks in the CMB.

O O O

Let us pause a while to discuss the results we have obtained so far.

Perhaps, the most dramatic result is expressed by Eq. (6.10), since it implies that the Universe is spatially *flat* – namely *euclidean* – in agreement with the natural expectation based on cosmic inflation [78]. Nevertheless, a warning is in order. Because the Einstein field equation tell us only about the *metric* properties, the *topology* of the Universe is totally unknown. Therefore, we should keep in mind that space can actually be topologically nontrivial, and so it can well happen that it is not flat but cylindrical.

Another remarkable fact is that the value of Ω_B – as given by Eq. (6.11) – fits within the range (6.1) even though it is quite close to the upper bound. Hence, we see that cosmology provides a solid prediction about the total amount of baryons in the Universe. Consequently, Eq. (5.9) implies

$$\Omega_M = 0.340 \pm 0.92, \quad (6.12)$$

in very good agreement with the result reported by the Planck collaboration [77]

$$\Omega_M = 0.308 \pm 0.012. \quad (6.13)$$

Usually, we are accustomed to think that galaxies are the building blocks of the Universe and the main place where matter is located. But this view must be wrong, since we have $\Omega_M = 0.308$ while we know that $\Omega = 1$. So, we are missing roughly two-third of the stuff the Universe is made of!

6.3 Accelerated cosmic expansion

The solution to this puzzle came in April 1997. Two independent collaborations, the Supernova Cosmology Project [79, 80] and the High-z Supernova Search Team [81, 82], reported that the observation of a set of Type Ia supernovae at cosmological distance implies that present Universe is undergoing an accelerated expansion.

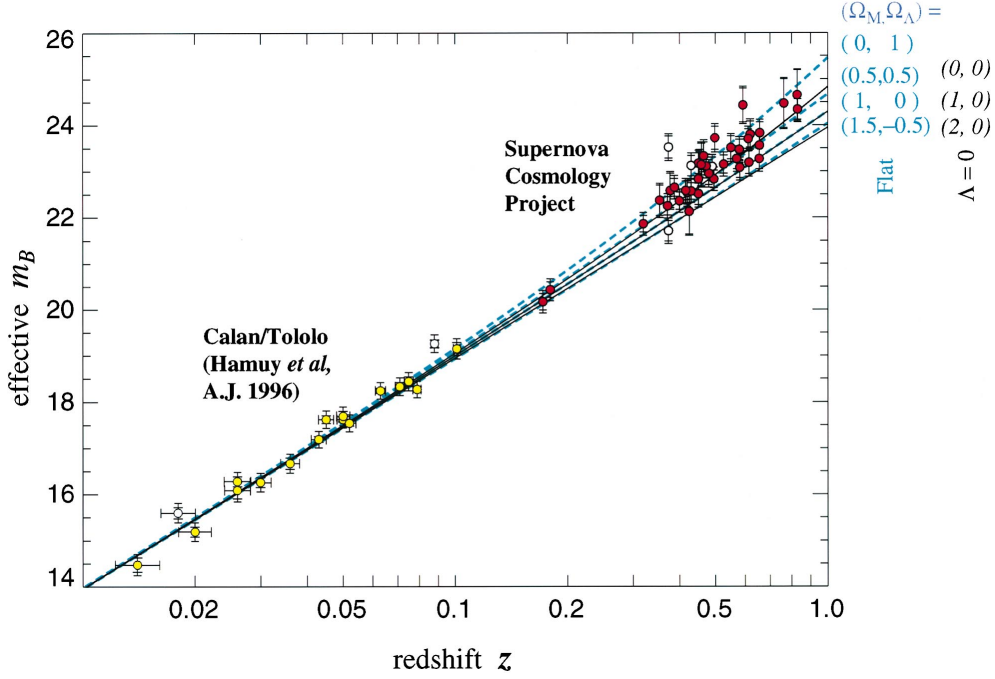


Figure 7: Hubble diagram for 42 high-redshift type Ia supernovae from the Supernova Cosmology Project and 18 low-redshift type Ia supernovae. The inner error bars show the uncertainty due to measurement errors, while the outer error bars show the total uncertainty when the intrinsic luminosity dispersion, 0.17 mag, of light-curve-width-corrected type Ia supernovae is added in quadrature. The unfilled circles indicate supernovae not included in fit C. The horizontal error bars represent the assigned peculiar velocity uncertainty of 300 km s^{-1} . The solid curves are the theoretical $m_B^{\text{eff}}(z)$ for a range of cosmological models with zero cosmological constant: $(\Omega_M, \Omega_\Lambda) = (0, 0)$ on top, $(1, 0)$ in middle, and $(2, 0)$ on bottom. The dashed curves are for a range of flat cosmological models: $(\Omega_M, \Omega_\Lambda) = (0, 1)$ on top, $(0.5, 0.5)$ second from top, $(1, 0)$ third from top, and $(1.5, -0.5)$ on bottom.

The idea goes back to Hubble, who realized that information about the geometry of the Universe can be obtained by observing *standard candles* located at cosmological distances. Accordingly, a measurement of the apparent luminosity (radiation flux) yields the *luminosity distance* while the redshift z is obtained by measuring that of the host galaxy. Because the luminosity distance depends not only on z but also on Ω_M and Ω_Λ , it follows that a curve in the plot of apparent luminosity versus redshift – the so-called *Hubble diagram* – is labelled by the pair $(\Omega_M, \Omega_\Lambda)$. Suppose now that both apparent luminosity (apparent magnitude) and redshift are measured for a sample of identical standard candles, chosen to be Type Ia supernovae. Accordingly, a curve in the

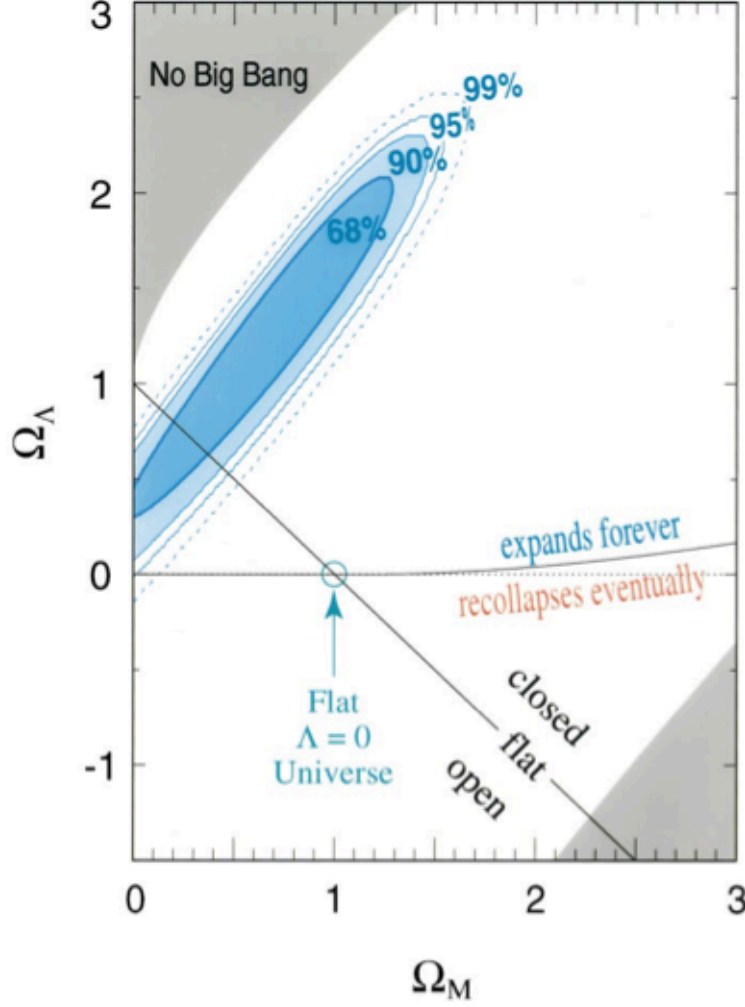


Figure 8: Best-fit confidence regions in the $(\Omega_M, \Omega_\Lambda)$ plane for our primary analysis. The 68%, 90%, 95%, and 99% statistical confidence regions in the $(\Omega_M, \Omega_\Lambda)$ plane are shown.

Hubble diagram gets singled out, and so a well-defined functional relationship between Ω_M and Ω_Λ emerges.

For instance, the Supernova Cosmology Project yields fit of the magnitude-redshift data for 42 Type Ia supernovae with $0.18 \leq z \leq 0.83$ plus another supernova survey with $z \leq 0.1$. Their results are exhibited in Figure 7. At the 99% confidence level their data imply that $\Omega_\Lambda > 0$, whereas their best fit gives

$$0.8\Omega_M - 0.6\Omega_\Lambda = -0.2 \pm 0.1, \quad (6.14)$$

which corresponds to major axis of the various blue ellipses in Figure 8. Correspondingly, the deceleration parameter q_0 reads

$$q_0 = -0.63\Omega_\Lambda - 0.13 \pm 0.06, \quad (6.15)$$

thereby implying that the present Universe is undergoing an accelerated expansion. For a flat

Universe they also report the age of the Universe $t_0 = 13.4_{-1.1}^{+1.4}$ Gyr as well as $\Omega_M \simeq 0.28$, as it can be seen from the intersection of the flat straight line corresponding to $\Omega_M + \Omega_\Lambda = 1$ with the ellipses corresponding to 68% confidence level in Figure 8.

Basically, the same conclusion has been reached by the High- z Supernova Search Team.

Now, by combining Eqs. (6.13) and (6.14) we get $\Omega_\Lambda = 0.74$, and so $\Omega = 1.05$, which is perfectly consistent with $\Omega = 1$ when errors are taken into accounts.

Thus, we conclude that the vacuum energy is just the missing stuff which fills the gap. As we have seen, having large negative pressure, it makes gravity repulsive. Moreover, it is self-repulsive, and so we expect to be spread out throughout the Universe without making structures. In addition, its contribution to galaxies and its clusters is irrelevant, thereby not upsetting our previous analysis.

7. Nature of dark matter

Finally, we briefly address the nature of dark matter as implied by the above analysis.

Baryonic dark matter: Our estimates of $\Omega_{\text{LUM}} = 0.0035$ and $\Omega_B = 0.049$ imply that more than 90% of the baryons do not emit light in the optical band. Surely, some of them are present in the intracluster region and emit X-rays. In addition, baryons constitute the so-called warm-hot intergalactic medium [83]. Nevertheless, a carefully inventory shows that about 50% of the baryons are dark, thereby giving rise to the problem of *non-baryonic dark matter* [57]. Their form is unknown. Still, several proposal have been made. For instance, it has been shown from a careful analysis of the formation process of the Milky Way and Andromeda that the observed properties can be reproduced only if 50 – 75% of the galactic baryons are dark [84]. In addition, it seem that the observed distribution of the rotation velocity of a statistically meaningful sample of spiral galaxies can be explained only if roughly 1/3 of the dark baryons lurk in galactic halos of spiral galaxies [85].

Non-baryonic dark matter: Clearly, $\Omega_M = 0.308$ exceeds $\Omega_B = 0.049$ by more than a factor of 6, thereby showing that this gives the leading contribution to the mass budget. Its need is absolutely compelling for the formation of structure in the Universe, provided it is *cold* (namely that it is non-relativistic when it decouples from the rest of the Universe) [86]. Unfortunately, their nature is totally unknown. The most popular candidates for cold dark matter are WIMPs (weakly interacting massive particles), which can be very heavy [87, 88]. Alternatively, cold dark matter can be made of very light particles, like axions [87] or axion-like particles (ALPs) [89, 90].

Dark energy: This is the stuff responsible for the *accelerated* cosmic expansion and described by $\Omega_\Lambda = 0.74$. Manifestly, this is the leading stuff in the Universe, and so we can well say that we do not have even the slightest idea concerning what the Universe is made of [91].

In conclusion, while all astrophysical and cosmological observation lead to results that numerically fit very nicely together, we still do not know the physical nature of the leading components of the Universe.

8. Acknowledgments

I would like to thank G. Galanti for a careful reading of the manuscript. I also thank the organizers for having invited me to give this talk in such a splendid environment.

9. Figure credits

Figure 2: Ref. [26].

Figure 3: <http://arxiv.org/abs/1503.02652>

Figure 4: NASA, ESA, Richard Ellis (Caltech) and Jean-Paul Kneib (Observatoire Midi-Pyrenees, France). Acknowledgment: NASA, A. Fruchter and the ERO Team (STScI and ST-ECF).

Figure: 5 Particle Data Group, IOP, K. Olive *et al.*, Chin. Phys. C **38**, 090001 (2014).

Figure: 6 <http://background.uchicago.edu/~whu/intermediate/intermediate.html>

Figure: 7 Ref. [79].

Figure: 8 Ref. [79].

References

- [1] J. C. Kaptein, *Astrophys. J.* **55**, 302 (1922).
- [2] J. H. Jeans, *Mon. Not. R. Astron. Soc.* **82**, 122 (1922).
- [3] J. H. Jeans, *Mon. Not. R. Astron. Soc.* **84**, 60 (1923).
- [4] J. H. Oort, *Bull. Astronom. Inst. Netherlands* **6**, 249 (1932).
- [5] J. H. Oort, *Bull. Astronom. Inst. Netherlands* **15**, 45 (1960).
- [6] J. I. Read, *J. Phys. G* **41**, 063101 (2014).
- [7] F. Zwicky, *Helv. Phys. Acta* **6**, 110 (1933).
- [8] F. Zwicky, *Astrophys. J.* **86**, 217 (1937).
- [9] P. Schneider, J. Ehlers and E. Falco, *Gravitational Lenses* (Springer, Berlin, 1992).
- [10] A. Einstein, *Science* **84**, 506 (1936).
- [11] F. Zwicky, *Phys. Rev.* **51**, 290 (1937).
- [12] F. Zwicky, *Phys. Rev.* **51**, 679 (1937).
- [13] B. Fort and Y. Mellier, *Astron. Astrophys. Rev.* **5**, 239 (1994).
- [14] M. Bartelmann and P. Schneider, *Phys. Rep.* **340**, 291(2001).
- [15] S. M. Kent, *Astrophys. J. Suppl.* **59**, 115 (1985).
- [16] K. C. Freeman, *Astrophys. J.* **160**, 811 (1970).
- [17] V. C. Rubin, D. Burnstein and N. Thonnard, *Astrophys. J.* **242**, L149 (1980).
- [18] V. C. Rubin, W. K. Ford and N. Thonnard, *Astrophys. J.* **253**, 471 (1980).
- [19] V. C. Rubin, W. K. Ford, N. Thonnard and D. Burnstein, *Astrophys. J.* **261**, 439 (1982).

- [20] V. C. Rubin, D. Burnstein, W. K. Ford and N. Thonnard, *Astrophys. J.* **289**, 81 (1985).
- [21] D. Burnstein and V. C. Rubin, *Astrophys. J.* **297**, 423 (1985).
- [22] S. M. Kent, *Astron. J.* **91**, 1301 (1986).
- [23] Y. Sofue and V. C. Rubin, *Ann. Rev. Astron. Astrophys.* **39**, 137 (2001).
- [24] A. Bosma, *Astron. J.* **86**, 1791 (1981).
- [25] A. Bosma, *Astron. J.* **86**, 1825 (1981).
- [26] T. S. van Albada, J. N. Bahcall, K. Begeman and R. Sancisi, *Astrophys.* **295**, 305 (1985).
- [27] J. Binney and S. Tremaine, *Galactic Dynamics*, Second Edition (Princeton University Press, Princeton, 2008).
- [28] M. Persic and P. Salucci, *Astrophys.* **368**, 60 (1991).
- [29] M. Persic, P. Salucci and F. Stel, *Mon. Not. R. Astron. Soc.* **281**, 27 (1996).
- [30] J. Bahcall and S. Tremaine, *Astrophys.* **244**, 805 (1981).
- [31] D. Lynden-Bell, R. D. Cannon and P. J. Godwin, *Mon. Not. R. Astron. Soc.* **204**, 87 (1983).
- [32] D. Zaritsky, R. Smith, C. Frenk and S. D. M. White, *Astrophys.* **478**, 39 (1997).
- [33] N. Bahcall, L. M. Lubin and V. Dorman, *Astrophys. J.* **447**, L81 (1995).
- [34] D. Lynden-Bell, *Mon. Not. R. Astron. Soc.* **136**, 101 (1967).
- [35] T. S. van Albada, *Mon. Not. R. Astron. Soc.* **201**, 939 (1982).
- [36] L. P. Osipkov, *Pis̄oma Astr. Zh.* **5**, 77 (1979).
- [37] D. Merritt, *Astron. J.* **90**, 1027 (1985).
- [38] O. E. Gerhard, *Mon. Not. R. Astron. Soc.* **265**, 213 (1993).
- [39] R. P. van der Marel and M. Franx, *Astrophys. J.* **407**, 525 (1993).
- [40] N. R. Napolitano *et al.*, *Mon. Not. R. Astron. Soc.* **393**, 329 (2009).
- [41] A. Kronawitter, R. P. Saglia, O. E. Gerhard and R. Bender, *Astron. Astrophys. Suppl.* **144**, 53 (2000).
- [42] O. Gerhard, A. Kronawitter, R. P. Saglia and R. Bender, *Astron. J.* **121**, 1936 (2001).
- [43] A. S. Bolton *et al.* *Astrophys. J.* **682**, 964 (2008).
- [44] R. Mandelbaum *et al.*, *Mon. Not. R. Astron. Soc.* **368**, 715 (2006).
- [45] R. Gavazzi *et al.*, *Astrophys. J.* **667**, 176 (2007).
- [46] M. Girardi *et al.*, *Astrophys. J.* **438**, 527 (1995).
- [47] R. Carlberg *et al.*, *Astrophys. J.* **462**, 32 (1996).
- [48] C. L. Sarazin, *Rev. Mod. Phys.* **58**, 1 (1986).
- [49] S. De Grandi and S. Molendi, *Astrophys. J.* **567**, 163 (2002).
- [50] A. Vikhlinin *et al.*, *Astrophys. J.* **628**, 655 (2005).
- [51] A. Vikhlinin *et al.*, *Astrophys. J.* **640**, 691 (2006).
- [52] H. Weyl, *Phys. Zeit.* 29, 230 (1923).

- [53] H. Hubble, Proc. Nat. Acad. Soc. 15, 169 (1929).
- [54] M. Carfore and A. Marzuoli, Phys. Rev. Lett. **53**, 2445 (1984).
- [55] T. Buchert *et al.*, arxiv: 1505.07800
- [56] P. Schechter, Astrophys. J. **203**, 297 (1976).
- [57] M. Fukugita, C. J. Hogan and P.J. E. Peebles, Astrophys. J. **503**, 518 (1998).
- [58] D. S. Madgwick *et al.*, Mon. Not. R. Astron. Soc. **333**, 133 (2002).
- [59] P. Norberg *et al.*, Mon. Not. R. Astron. Soc. **336**, 907 (2002).
- [60] M. R. Blanton *et al.*, Astron. J. **121**, 2358 (2001).
- [61] B. Tinsley, Astrophys. J. **241**, 41 (1990).
- [62] M. Postman and M. J. Geller, Astrophys. J. **281**, 95 (1984).
- [63] S. D. M. White, J. F. Navarro, A. E. Evrard and C. S. Frenk, Nature **366**, 429 (1993).
- [64] P. A. R. Ade *et al.* [PLANCK collaboration], Astron. Astrophys. **571**, 16 (2014).
- [65] G. Steigman, Annu. Rev. Nucl. Part. Sci. **57**, 463 (2007).
- [66] M. Rauch *et al.*, Astrophys. J. **489**, 1 (1998).
- [67] P. D. Naselsky, D. I. Novikov and I. D. Novikov, *The Physics of the Cosmic Microwave Background* (Cambridge University Press, Cambridge, 2006).
- [68] R. Durrer, *The Cosmic Microwave Background* (Cambridge University Press, Cambridge, 2008).
- [69] S. Weinberg, *Cosmology* (Oxford University Press, Oxford, 2008).
- [70] M. Giovannini, *A primer on the Physics of the Cosmic Microwave Background* (World Scientific, Singapore, 2008)
- [71] P. De Bernardis *et al.* [BOOMERANG collaboration], Astrophys. J. **564**, 559 (2002).
- [72] A. Balbi *et al.* [MAXIMA collaboration], Astrophys. J. **545**, L1 (2000).
- [73] C. Pryke *et al.* [DASI collaboration], Astrophys. J. **568**, 46 (2002).
- [74] C. L. Bennet *et al.* [WMAP collaboration], Astrophys. J. **583**, 1 (2003).
- [75] W. Hu, N. Sugiyama and J. Silk, Nature **386** (1997) 37.
- [76] U. Seljak and M. Zaldarriaga, Astrophys. J. **469**, 437 (1996).
- [77] P. A. R. Ade *et al.* [PLANCK collaboration] arxiv:1502.01589
- [78] A. R. Liddle and D. H. Lyth, *Cosmological Inflation and Large-Scale Structure* (Cambridge University Press, Cambridge, 2000).
- [79] S. Perlmutter *et al.*, Astrophys. J. 517, 565 (1999).
- [80] S. Perlmutter *et al.*, Nature 391, 51 (1998).
- [81] A. G. Riess *et al.*, Astron. J. 116, 1009 (1998).
- [82] B. Schmidt *et al.*, Astrophys. J. 507, 46 (1998).
- [83] A. Bykov, F. B. S. Paerels and V. Petrosian, Space Science Review **134**, 141 (2008).
- [84] A. Klypin, H. S. Zhao and R. Somerville, Astrophys. J. **573**, 597 (2002).

- [85] C. S. Hocheanek and M. White, *Astrophys. J.* **559**, 531 (2001).
- [86] M. S. Longair, *Galaxy Formation*, Second Edition (Springer, Berlin, 2008).
- [87] *Particle Dark Matter*, edited by G. Bertone (Cambridge University Press, Cambridge, 2009).
- [88] M. Taoso, G. Bertone and A. Masiero, *JCAP*, **03** 022 (2008).
- [89] A Ringwald, contribution to these Proceedings.
- [90] P. Arias *et al.*, *JCAP*, **06** 008 (2012).
- [91] L. Amendola and S. Tsujikawa, *Dark Energy* (Cambridge University Press, Cambridge, 2010).